QATAR UNIVERSITY

COLLEGE OF ENGINEERING

INHIBITION OF INORGANIC OILFIELD SCALES: THEORETICAL INVESTIGATION

BY

MOHAMMAD J. AL ABD AL HAMAD

A Thesis Submitted to

the College of Engineering

in Partial Fulfillment of the Requirements for the Degree of

Masters of Science in Environmental Engineering

January 2021

COMMITTEE PAGE

The members of the Committee approve the Thesis of

Mohamma J. Al Abd Al Hamad defended on 29/11/2020.

_____

Prof. Majeda Khraisheh
Thesis/Dissertation Supervisor

_____

Prof. Ibnelwaleed A. Hussein
Thesis/Dissertation Co-Supervisor

_____

Prof. Ramazan Kahraman
Committee Member

_____

Dr. Zeinab Abbas Jawad
Committee Member

Approved:

_____

Khalid Kamal Naji, Dean, College of Engineering

ABSTRACT

Mohammad, Al Hamad, J., Masters: January: 2021, Masters of Science in Environmental Engineering

Title: Inhibition of Inorganic Oilfield Scales: Theoretical Investigation

Supervisor of Thesis: Prof. Majeda Khraisheh, Co-supervisor of Thesis: Prof. Ibnelwaleed A. Hussein

Scale deposition is a critical issue in the oil and gas exploration and production processes causing significant blocking in the tubing and consequently flow assurance and economic losses. Most studies addressing the scale formation have focused on the experimental impact of different variables on scale formation. At the start of this work, the formation and inhibition of inorganic oilfield scales such as iron sulfide, calcite, and barite scales theoretically was analyzed by using Density-Functional Theory (DFT) simulation. Molecular dynamics simulation and DFT calculation were used to investigate the inhibition effects of four different scale inhibitors polyacrylic acid (PAA), hydrolyzed polymaleic anhydride (HPMA), polyepoxysuccinic acid (PESA) and polyaspartic acid (PASP) on iron sulfide scale formation. After that, the inhibition of barite scale deposition was investigated by employing molecular simulation (VASP and DFT) for three different scale inhibitors namely: (Polyaspartic acid, PASP; Nitrilotrimethylenephosphonateand, NTPM; Dimethylenetriaminepenta (methylene-phosphonic acid), DETPMP). The selected inhibitors are widely used in the industry. Geometrical analysis were used to explore the inhibitors performance and visualize the outcomes. QSAR parameters were also used to predict the activity of the inhibitors in the system. . Binding energy calculation produced -

1.06 eV, -0.17 eV, and -2.33 eV for PASP, NTPM, and DETPMP, respectively. The results of this study indicated that the inhibition strength of the three inhibitors on barite scale formation can be sequenced as DETPMP>PASP>NTPM, which is in agreement with experimental observations. Moreover, the ecological toxicity properties were predicted, and the environmental impact of the different inhibitors assessed. All inhibitors showed comparable eco-tox properties, and predicted to be soluble in water. Molecular simulations proved to be an effective tool in the prediction of the performance and toxicity of barite scale inhibitors.

Key Words**:** Barite scale; scale inhibitors; Density functional theory; QSAR Parameters; Eco-tox Properties; Geometrical Analysis

DEDICATION

I dedicate this work to my parents, my wife, and my sisters for their endless support. In addition, I dedicate this work to my academic advisors, Prof. Majeda Khraisheh, and Prof. Ibnelwaleed A. Hussein for their academic support.

ACKNOWLEDGMENTS

I would like to express my gratitude to my supervisors, Prof. Majeda Khraisheh, and Prof. Ibnelwaleed A. Hussein for their academic support. Without their help, the objectives of this project would not have been achieved. In addition, I would like to recognize the priceless assistance from my colleague Mr. Abdulmujeeb Toluwase Onawole and Dr. Saad Ali S S Al-Sobhi. I would like to also acknowledge the infrastructure and support of the Chemical Engineering Department, College of Engineering, and Gas Processing Center at Qatar University and all its members. Finally, I am indebted to my family for their support and motivation during my graduate education.

TABLE OF CONTENTS

LIST OF TABLES

LIST OF FIGURES

Chapter 1: Introduction

1.1 Research Overview

Many challenges can have an impact on the oil and gas exploration and production wells including scale formation and considered as one of the most severe oilfield problems. Scale is the accumulation of different minerals at the subsurface of the wells and tubes that may lead to clogging in the wellbore, production tubing, and downhole tubulars [1]. Scale formation leads to financial losses, which prompted a great interest from the oil and gas industry and the research community to address its causes and associated impacts. Scale inhibitors are chemicals that can be used to prevent or slow scale formation in oil and gas wells. Scale inhibitors are used as a primary control method for oilfield scale. In some cases, scale inhibitors are not effective in preventing the scale formation, such as when the inhibitors is not placed optimally inside the well, and when the scale formation is not predicted accurately in reservoir conditions [2]. Scale inhibitors can be classified into many classes, such as including phosphorous as scale inhibitors [3], [4], green scale inhibitors [5], and polymers as scale inhibitors [6]. Moreover, inhibitor coordination group selection is essential parameter as scale inhibitors compounds with more than one lone pair of electrons can have better inhibition properties [7].

The understanding of scale formation mechanisms and the identification of the different types of scale formation are pivotal for the control of such occurrence in the oil and gas industry [8]. It is reported that scales can deposit in many forms and in different locations in the well, for example iron sulfide can deposit near the wellbore region, downhole and topside tubes of the well in addition to the sides of the reservoir [9]. Different wells may have scales that are different in composition, severity, and depth. For example, at around

6000 ft on the downhole tubing, the scale starts to be noticeable, and the severity increases as the depth increases [10].

Several factors influence the deposition of scale inside the reservoir and wells. In general, the main factors that affect scale formation are temperature, pH, operating pressure, flow velocity, permeation rate, salt content, and the presence of other metal ions in the system [11]. From a thermodynamic point of view, precipitation becomes feasible when the solution is supersaturated and ions in solution are higher than their saturation limit. The severity of scale is impacted by the kinetics of precipitation [12]. Many studies were conducted to evaluate scale types in the oil and gas industry [13], [14]. In general, scales are composed of sulfate, phosphates, carbonates, and other general forms, such as alumina silicates [15]. Common scale types include different forms of iron sulfides and ferric compounds depending on reservoir conditions [3]. However, the most common scale types detected are barite, calcite $CaCO_3$, gypsum $CaSO_4.2H_2O$, and dolomite $CaMg(CO_3)_2$.

Figure 1 shows typical scale deposition in pipelines. It can be notice that how deposition of scale can influence the pipelines. However, this is a small example, while in reality; scale damage can be much greater.

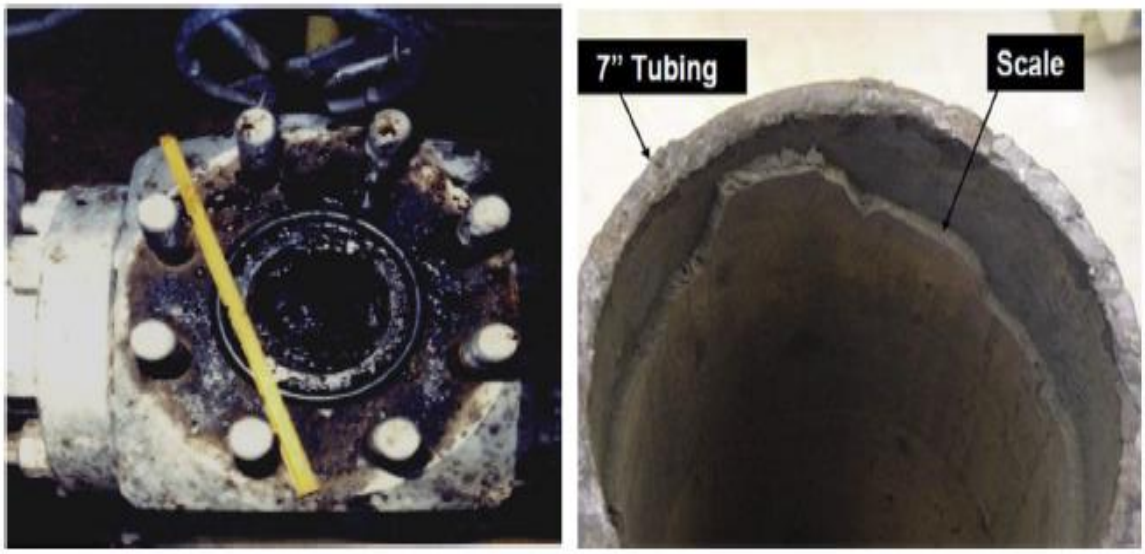

Figure 1. Typical scale deposition example [16]

The source of barite in oil and gas wells is typically related to the drilling fluids, and barite scales are one of the toughest scale types to be handled [17]. A study to explain the effect of pH on the dissolution of iron sulfide scales by using tetrakis (hydroxymethyl) phosphonium sulfate (THPS) was performed [18]. A computational study was applied to analyze the effect of pH on acidic and basic chelating agents used in the removal of iron sulfide scales [19]. Barite scale is affected by changing the pH of the solution. Particularly the nucleation and growth rates of barite scale can be influenced by changing pH. Nanoscale Atomic Force Microscopy (AFM) study shows that barite nucleation and growth rates are encouraged clearly in range of 9-12 pH at alkaline region [20]. Moreover, pH is a critical variable for scale inhibition, and pH can affect the barite scale inhibitors efficiency. The effect of pH on barite scale inhibition efficiency (IE) for different scale inhibitors such

as DETPMP were reported [21]. For Dimethylenetriaminepenta (methylene-phosphonic acid) (DETPMP), increasing the pH promotes the inhibitor efficiency (IE), and the optimum pH for DETPMP for barite inhibition was detected to be 6.5 [21]. An active formulation for the removal of barite scale by using chelating agents and catalyst is studied [22], and the optimum concentrations for chelating agents and catalyst to dissolve barite scale are obtained.

Experimental evaluation of the performance of many potential inhibitors is costly and lengthy. However, applying simulation techniques and thoertical studies saves money and time. Moreover, thoertical studies contribute in the understand of the governing mechanisms of such inhibition processes and help in verifying experimental data. In this study, the theoretical tools are employed to predict the ability of three commercial chemicals to inhibit the formation of barite scale under typical field conditions. The outcomes of the theoretical calculations on the inhibition performance of the three inhibitors (PASP, NTMP, and DETPMP) are tested against reported experimental data.

In this work, scale inhibitors are theoretically studied using Density-Functional Theory (DFT) to understand the mechanisms of barite scale inhibition. The chemical name and formula of the three inhibitors (PASP, NTMP, and DETPMP) are shown in Table 1. Whiile for iron sulfide and calcite scale inhibition calculation, Polyepoxysuccinic Acid (PESA), Hydrolyzed Polymaleic Anhydride (HPMA) and Polyaspartic Acid (PASP) classical inhibitors were used.

The compounds selected for studying the inhibition effect of barite scale are conventional inhibitors that are widely used for barite scale inhibition investigations [23]–[25]. Three different commercial inhibitors were selected for the simulation study to evaluate and

compare their performance. Table 1 shows the chemical name and formula of the inhibitors used in this study. The density for inhibitors are obtained directly from Advanced Chemistry Development ACD/Labs Chemsketch software [26] , and the density values are at standard conditions (297.15 K, and 1 atm).

Table 1. Chemical name and formula of scale inhibitors

Inhibitor	Chemical Name	Formula
PASP	Polyaspartic acid	$C_8H_{12}N_2O_7$
NTPM	Nitrilotrimethylenephosphonateand	$C_3H_{12}NO_9P_3$
DETPMP	Dimethylenetriaminepenta (methylene-phosphonic acid)	$C_9H_{28}N_3O_{15}P_5$

1.2 Objectives

The objectives of this study are as follows:

1- To investigate the inhibition of inorganic oilfield scales theoretically by using molecular dynamics simulation techniques.

2- To examine and compare the inhibition performance of conventional oilfield scale inhibitors used in this study (PASP, NTMP, and DETPMP) by using different criteria such as binding energy calculations and graphical analysis.

3- To investigate the ecological toxicity properties and the environmental impact of the different inhibitors used in this study. Moreover, QSAR parameters calculation were applied, QSAR corresponds to the Quantitative Structure-Activity Relationship. This technique is used to predict the activity and reactivity of molecules on a system based on a set of equations and analyzing the resulted behavior.

1.3 Research Contribution

Current practice in scale inhibitors evaluation by experimental procedures of the performance of several oilfield scale inhibitors is costly and time consuming. So conduct theoretical and modeling studies benefit understand the main mechanisms of such inhibition and help verify experimental data. In addition, thoertical evaluation of inhibitiors performance can save time and money. Molecular dynamics techniques such as The Vienna Ab initio Simulation Package (VASP) version 5.4.4. code and Density-Functional Theory (DFT) was used for all calculations in this study. The result obtained in this study was compared with expermental findings and shows agreement. This suppports one of the objectives of this work mentioed eralier, that thoertical studies can svae time and money and yield resnoaible and reliable data. Binding energies calculation were used to evaluate the binding strength of each inhibitor with the scale surface. Geometrical analysis were applied to investigate the inhibitors performance and visualize the outcomes between the inhibitors and scale surface slab. Moreover, the Quantitative Structure-Activity Relationship (QSAR) was utilized to predict the activity and reactivity of inhibitors on the system. The results of this study indicated that the inhibition strength of the three inhibitors on barite scale formation can be sequenced as DETPMP> PASP> NTPM, which is in agreement with experimental observations.

1.4 Research Outcome

1- **Mohammad Al Hamad**, S. A. Al-sobhi, A. T. Onawole, I. A. Hussein, and M. Khraisheh, “Density-Functional Theory Investigation of Barite Scale Inhibition Using Phosphonate and Carboxyl-Based Inhibitors,” 2020. ACS Omega 2020 5 (51), 33323-33328. DOI: https://doi.org/10.1021/acsomega.0c05125

Chapter 2: Literature Review

Scale deposition is a critical issue in the oil industry, scale depositions occurs when the process conditions help in creating the super saturation state for one of scale-type soluble salts. Snowballing environmental concerns have caused researchers to scope scale inhibition and removal more and more. This section reviews the recent reported types of scale, factors affecting their formation, scale inhibition, and scale removal.

2.1 Types of Scale in oil and gas fields

Oilfield scales studies discovered many types of scale. Common oilfield scales includes sulphides, carbonates, sulfates, iron scales, and miscellaneous [1]. Moreover, scale types include different forms of iron sulfides such as (mackinawite FeS, pyrrohtite $Fe_{1-x}S$, troilite FeS, pyrite FeS_2, greigite Fe_3S_4), ferric compounds as well (magnetite Fe_3O_4 and hematite Fe_2O_3), ferrous compounds such as (hibbingite $Fe_2(OH)_3Cl$, and wustite FeO). Iron sulfide present in many crystalline forms and shapes depending in sulfur to iron ratio, and conditions changes can produce other types and form of iron sulfide scale [3]. Moreover, there are common types were detected such as barite, calcite $CaCO_3$, gypsum $CaSO_4.2H_2O$, and dolomite $CaMg(CO_3)_2$. In general, scales are composed of sulfate, phosphates, carbonates, and other general forms such as alumina silicates [15]. Figure 2 summarizes the main and important common oilfield scales.

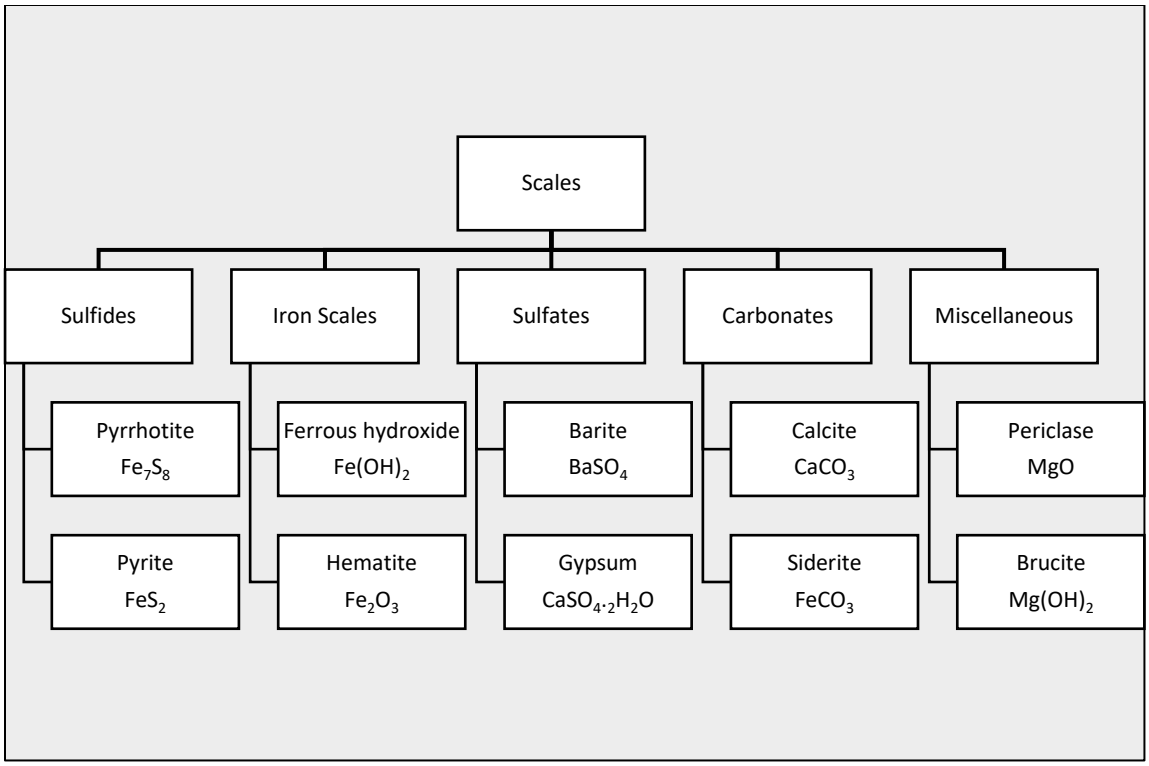

Figure 2. Common oilfield scales

A study that shows the variety of scale types collected 90 samples from 37 sour gas wells in Khuff reservoir are collected and analyzed by X-ray diffraction (XRD) [10]. From these samples, a wide range of scale kinds has been identified; Figure 3 displays the presence and relative abundance of the identified oilfield scale minerals. Figure 3 (A) illustrate the number of occurrences of different scale types, and Pyrrhotite scale comes first with 88 occurrences from these samples. Figure 3 (B) illustrates the average wt% for each mineral in the analyzed samples, and again Pyrrhotite dominates with around 46.8 wt%. and the last part Figure 3 (C), shows the maximum wt% for each mineral in a sample, and Pyrrhotite scale has the highest value with 93%. This means in this Khuff reservoir, Pyrrhotite scale dominates inside the well.

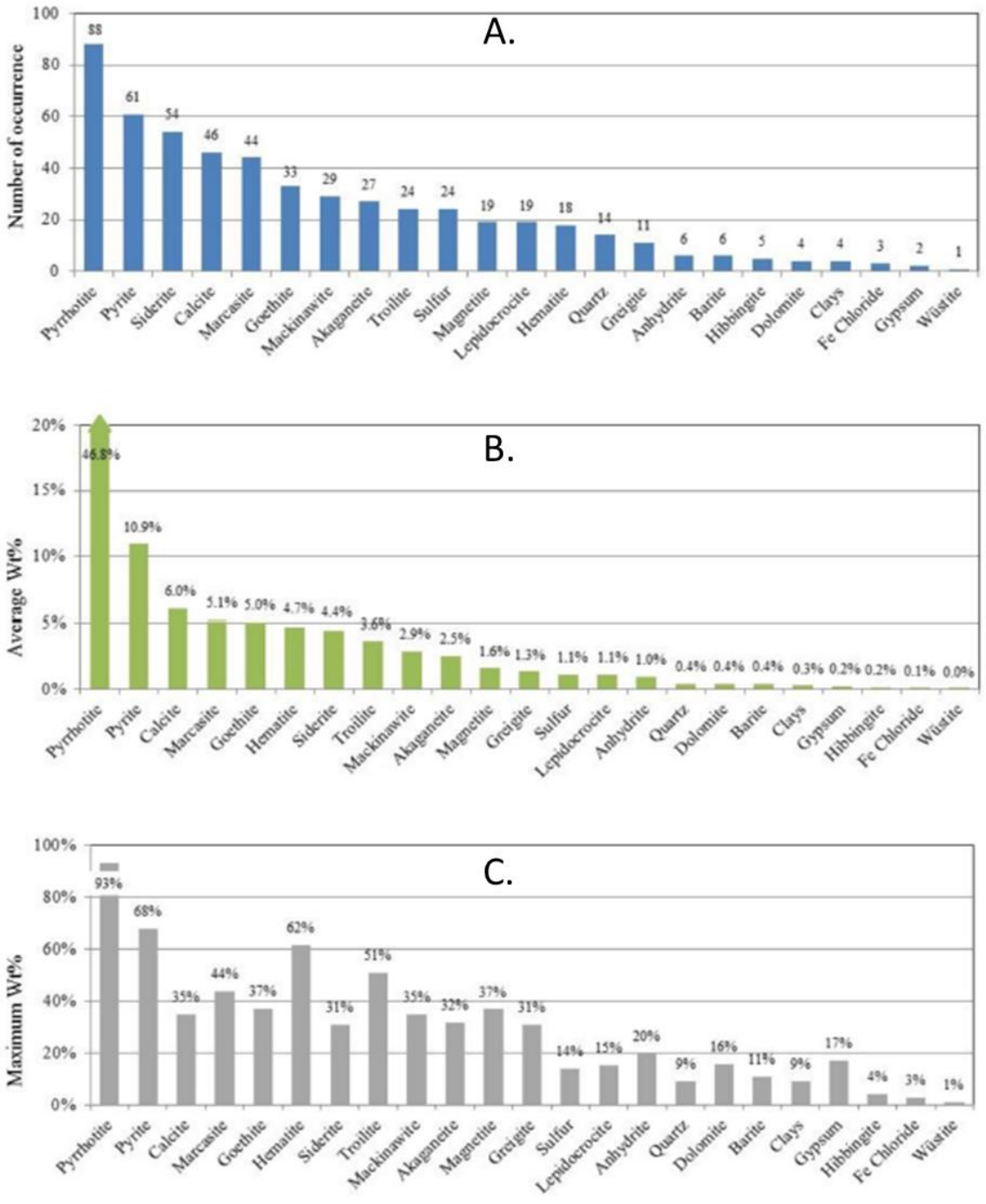

Figure 3. Appearance and relative abundance of the identified oilfield scale minerals [10]

2.2 Factors affecting scale formation

Deposited scale inside reservoirs is influenced by many factors. From thermodynamic point of view, precipitation becomes feasible when the solution is supersaturated and ions in solution are higher than their saturation limit, and the severity of scale is impacted by the kinetics of precipitation [12]. In general, the main factors that affect scale formation reported to be temperature, pH, operating pressure, flow velocity, permeation rate, salt content, and the attendance of other metal ions in the system [11], [27].

Solid scales only formed at pH≥4.5 at study condition. Increasing the pH and salinity has a negative effect on the performance of scale inhibitors [28]. A static test procedure for metal sulfide scale prediction and inhibition has been developed and various chemistries were tested for iron sulfide scale inhibition [29]. The oilfield conditions can be simulated in the lab to study the scale formation and control. In addition, it shows that surface treatment can be a method to prevent minerals scale deposition in water re-injection lines [30]. A Pressure/Volume/Temperature (PVT) software package and scale-prediction modelling techniques was combined to provide accurate scaling profile by using in-situ pH and water compositions, to produce how to find the maximum concentration of dissolved iron which is stable at given conditions in the reservoir [31].

The concentration of the mineral inside the reservoir plays a critical role in the scale deposition process. The concentration of $CaSO_4$ was changed gradually (from 500 ppm to 1500 ppm) while keeping other factors as constant. From Figure 4, it is clear that there is a direct relation between salt concentration and the scale deposition weight. However, this increase in scale deposition as concentration increases was expected, since the supersaturation of the salt is main driving force for scale formation [32].

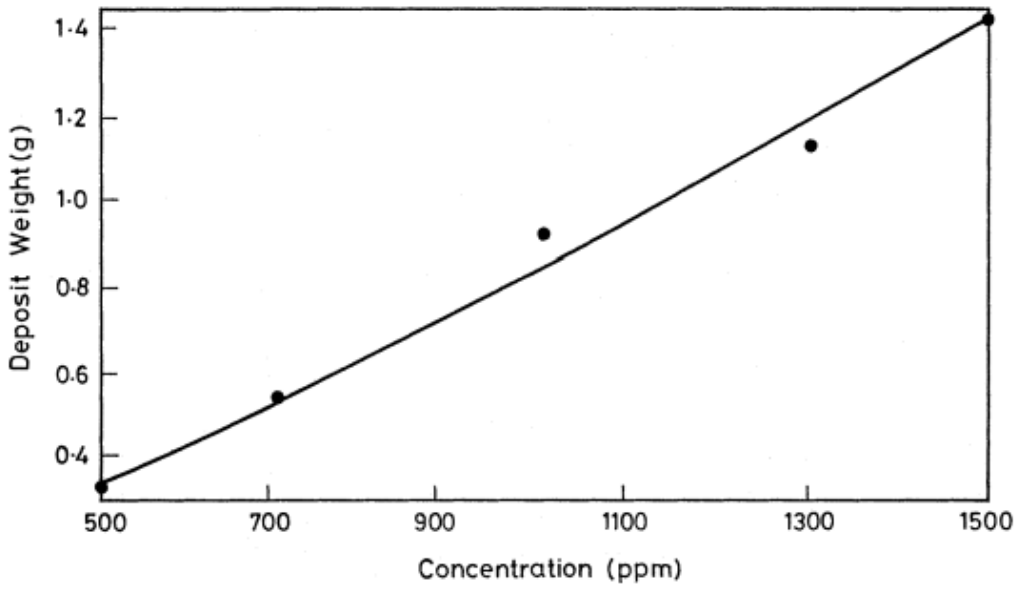

Figure 4. CaSO4 Concentration (ppm) Vs Deposition weight (g) [32]

Moreover, the temperature is one of the main factors that affect scale formation, since it is also has a direct effect on the supersaturation concentration of the salts inside the system. Figure 5 shows the effect of temperature on the $CaSO_4$ scale deposition, and it is clear that as temperature increases scale deposition weight increases as well [32].

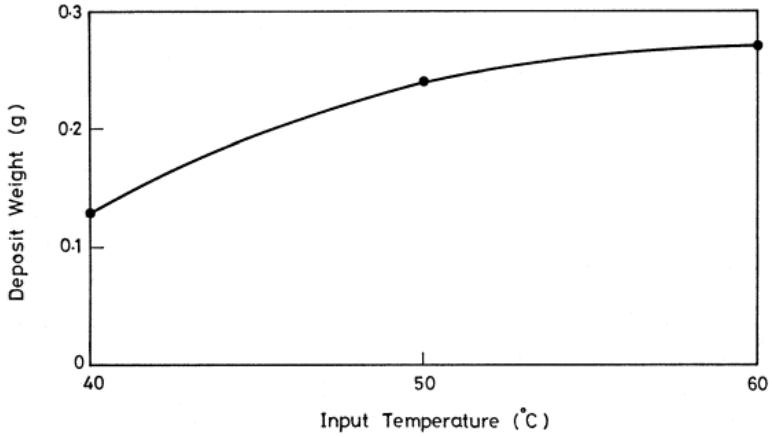

Figure 5. Effect of temperature on scale deposition [32]

2.3 Iron Sulfide Scale Formation Mechanism

Iron sulfide scale is a major scale types that mostly form in sour oil and gas wells. Iron sulfide scale formation is a function of temperature, pH, and pressure. Iron sulfide formation take place because of the reaction between iron and hydrogen sulfide H_2S. Hydrogen sulfide is able to react under reservoir conditions with ferric iron ion Fe^{+2} and cause iron sulfide scale deposition. The main source of reactant hydrogen sulfide is production of hydrogen sulfide as free gas in major of sour wells. However, there are other sources such as sulfate reducing bacteria (SRB), thermal degradation of drilling mud, and thermochemical sulfate reduction (TSR) inside the well. Moreover, the iron is mainly produced from the leaching of iron ions from minerals that are present in the system of the well, and as a product of corrosion of the tubulars. Other iron sources can be from minerals, propping agents, tubes of the equipment, clays, and formation brine [33]. Iron sulfide scale can precipitate near wellbore area, topside pipelines, and along the entire equipment. The formation reaction of iron sulfide scale is as the following reaction:

$$xFe^{+2} + yH_2S \rightarrow Fe_xS_{y(S)} + yH_{2(g)}$$ [13]

Scales usually differs from well to another; especially iron sulfide scales had a wide range of forms depending on the conditions in the reservoir and other factors such as iron to sulfur ratio. Moreover, inside the same well sometimes, many forms of iron sulfide scale can present and this is mainly depending on how deep is the reservoir. One way to prevent or mitigate the iron sulfide scale formation is to remove one of the components of the reaction from the system. Hydrogen sulfide in the production system from sulfate reducing bacteria (SRB) and thermochemical sulfate reduction (TSR) present in very high amount, which lead to be economically not logical to remove it from the system as a way of mitigation to

iron sulfide scale problem [34]. However, mitigation methods should focus on minimizing the sources of the reactant in the system, prevent and control the formation of iron sulfide precipitate inside the well, and lastly remove and deposited layers of iron sulfide scale as last measure of treatment.

Figure 6 illustrate some of the common reaction pathways for iron sulfide scale formation [10].

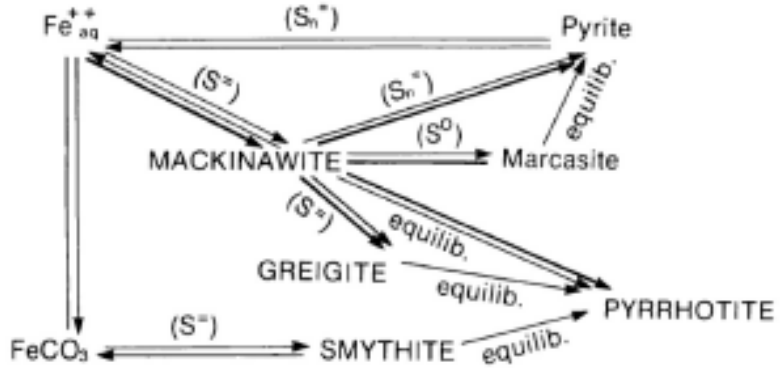

Richard
(1969)

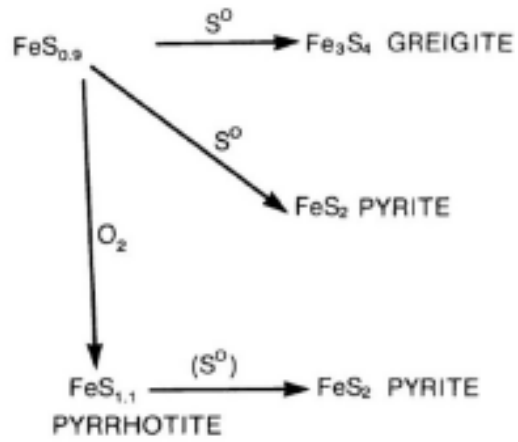

Sweeney and Kaplan
(1973)

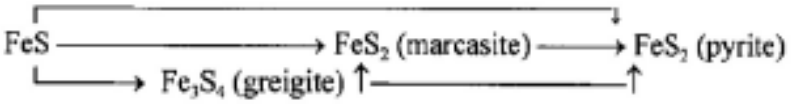

Anderko and Shuler
(1997)

Figure 6. Reaction pathways for some of iron sulfide scale [10]

2.4 Scale Inhibition

Scale inhibitors are chemicals that can be used to prevent or slow scale formation in oil and gas wells. Scale inhibitors are used as a primary control method for iron sulfide scale. In some cases, scale inhibitors are not effective in preventing the scale formation, such as when the inhibitors is not placed optimally inside the well, and when the scale formation is not predicted accurately in reservoir conditions [2]. Moreover, inhibitors are used to minimize the scale formation, but once the scale deposited it needs to be removed by scale removals or dissolvers. Some common antiscalant addition or scale inhibitors are listed below.

2.4.1 Inhibitor Coordination Group Selection

Compound that has lone pair of electrons are considered to have a better chelation characteristic. Therefore, scale inhibitors compounds with more than one lone pair of electrons can be better scale inhibitors. The properties of inhibitors coordination group help in determining inhibitor based group for each type of scale. Some common coordination group with their properties are shown in Table 2.

Table 2. Common coordination groups with their properties [7]

Group	Properties
—COOH	Hydrophilic, appropriate water solubility. Increase the solubility in water for metal ions, and boost the scale inhibition and removal processes.
—OH	Hydrophilic, it has electrons lone pair. It also increases solubility of particles in the water system.
—SO_3H	Solid polar groups, dissolves in polar solvents easily, and water-soluble.
—NH_2	Hydrophilic, it has electrons lone pair, also it improves solubility of particles in the water system.
—COOR	Resistance of polymers in the condensed action groups, high adsorption potential, it can modify the scale removal process.

2.4.2 Including Phosphorous as Scale Inhibitors

There are two class for scale inhibitors that include phosphorous in their structure which are polymeric phosphate and non-polymeric phosphate. Scale inhibitors containing phosphate can control the crystal growth of the scale. Such inhibitors can be used for a large range of pH values, and they have good chemical stability. For oil and gas wells scale deposited, the second class non-polymeric inhibitors containing phosphate can perform better than polymeric class, especially for calcite $CaCO_3$ and the barite $BaSO_4$ scales [3]. For non-polymeric phosphate scale inhibitors, there are some common types used widely for example: amino trimethylene phosphonic acid (ATMP), 2-phosphonobutane-1,2,4-tricarboxylic acid (PBTCA), methyl amino dimethylene phosphonic acid (MADMP), hydroxy,1-hydroxyethylidene-1, diethylene triamine penta (methylene phosphonic acid) (DETPMP), hexamethylene diamine-N,N,N',N'-tetra kis (HDTMP), 1-diphosphonic acid (HEDP), and ethylene diamine tetra methylene phosphonic acid (EDTMPA) [4]. Polymer inhibitors containing phosphate for scale inhibition are manufactured by inorganic monomer phosphate, and some other organic monomers can be used as well in synthesizing these kinds of inhibitors.

2.4.3 Green Scale Inhibitors

Polyaspartic acid (PASP) is one of the most synthesized green inhibitors [35], combined with other artificial inhibitors such as polyepoxysuccinic (PESA) [5]. Moreover, PASP and PESA are verified worldwide to be high effective green inhibitors for scale of oil and gas wells. Green scale inhibitors area needs more development and advanced investigation, since some other regular inhibitors have adverse impact on the environment.

2.4.4 Polymers as Scale Inhibitors

In research field, polymers are used in many applications to develop compounds or chemicals that can minimize the problem of that application. For scale inhibition applications, developed polymers such as polyacrylates are the most commonly used in scale inhibitors field since it has high inhibition efficiency and environmental impact [6]. Recently, the modern polymer inhibitors are begin used widely in oil and gas wells such as carboxylic acid polymer, phosphorus containing polymer scale inhibitors, and sulfonic acid-based polymer.

2.5 Scale Removal

After utilizing scale inhibitors as a control measure, scale dissolvers or removal is used to minimize the effect of iron sulfide scale. There are both chemical and mechanical methods to remove the deposited iron sulfide scale in oil and gas wells. Economics, damage to wellbore region tubing, fast and efficiency are all critical aspect while dealing with scale removal. Mechanical methods are applicable if the scale is formed in wellbore and can be removed out easily, but it should be accessible to be removed by mechanical means. Mechanical methods cannot be applied if the scale is present in the formation. In addition, using mechanical methods usually is expensive compared to chemical methods and this is due to the complex drilling process and its sequences.

Chemical methods are considered cost-effective compared to mechanical methods. Chemical methods can be used to remove the scale for both wellbore region and formation. There are so many types of chemicals can be used such as organic and inorganic chemicals to remove the scale. The optimum scale dissolver can be selected after analyzing the scale deposited inside the well, by studying the composition of the scale formed and its chemical

and physical characteristics. Since scale formed is different from one well to another, scale dissolvers also are different for each well because of diverse nature of scales. However, if the chemical dissolvers are selected poorly, they increase the recurrence of iron sulfide scale. Some example of scale dissolvers is listed below.

2.5.1 Hydrochloric Acid HCL

Hydrochloric acid is one of the most common scale dissolvers that are used to remove scale in oil and gas exploration industry. Hydrochloric acid is powerful scale dissolver since the majority of the scale minerals have high solubility in acids. In addition, using HCL dissolver at extremely high temperature can very costly, since many extra additives are required to control the reaction [8]. For iron sulfide scale, hydrochloric acid can remove few of them such as pyrrohtite and troilite, while pyrite and marcasite are hard to be removed by HCL. For other scale types such as zinc sulfides thy can dissolve in hydrochloric acid but other dissolver can achieve better results. The main point is that for each case, the better dissolver is different depending in many factors stated earlier. Hydrochloric acid can dissolve specific types of scale and ineffective in dissolving other, for example it can remove FeS from the reservoir, but it's not applicable in dissolving FeS_2 [36]. Hydrochloric acid dissolver is considered cost-effective and achieve very high performance for plenty of scale types, but the negative impact on the environment is an issue which needs a better control before the application of hydrochloric acid dissolver. Hydrochloric acid remover can generate hydrogen sulfide H_2S from the system and it can cause corrosion which are both not environmental impacts. In addition, hydrogen sulfide scavengers is typically must be used when using hydrochloric acid to control and prevent the free H2S gas generated in the dissolving process by using hydrochloric acid [37].

2.5.2 Chelating Agents

Chelating agents are compounds that have electron-donating group; this carbon-donating group can form a coordination bond with metal ion. The process of chelating can be described simply as the chelating agent are negatively charged which can sequestrate metal ions that are positively charged through chelation process. The chelating agent work by forming ring structures that have the ability to capture most of the coordination sites of the metal ions, and this cause's lower interaction between the metal ions and other ions in the system. One critical parameter in chelation process is the stability constant, which indicates the affinity of chelating agent for metal ion. Size of the ring, number of rings, pH of the chelating agent are examples of the factors that affect the stability constant [38]. Comparing to HCL dissolver, chelating agents have lower corrosion rate. In addition, chelating agents are considered an attractive alternative to inorganic and organic acids for dissolving scale in formation region. Chelating agent are less corrosive to downhole equipment and reservoir tubular, more environmental friendly, and easily biodegradable. In other hand, with all these advantages, compared to inorganic acids chelating agent still have higher cost [39]. Some of the common chelating agents comprise ethylenediamine tetraacetic acid (EDTA), hydroxyethyl iminodiacetic acid (HIDA), hydroxyethyl ethylene diamine tetraacetic acid (HEDTA), Diethylene triamine pentaacetic acid (DTPA), Methylglycinediacetic acid (MGDA), Nitrilotriacetic acid (NTA), and L-Glutamic acid N N-diacetic acid (GLDA) [39].

2.5.3 Organic acids

Organic acids are used also as alternative to HCL dissolver in some cases, for example high temperature high pressure (HTHP) systems. Common organic acids dissolvers are formic acid, maleic acid, acetic acid, and citric acid. However, its reported that HCL dissolver have higher dissociation constants compared to many common organic acid dissolvers [40]. A mixture of organic and inorganic acids can be used as effective dissolver for high temperature carbonate formation. However, organic acids considered as not effective dissolvers in removing the common types of iron sulfide FeS scale such as pyrite at various conditions of temperature and pH.

2.6 Scale Challenges

During last few years, huge number of studies investigated the formation of scale, as well as inhibition and removal of scale in gas exploration processes. The scope of the majority of the work done on scale area was about conventional mineral scale in oil and gas wells such as calcium carbonate scales, and calcium sulfate scales. While iron sulfide scale received lower attention compared to other conventional scales in terms of study and conducting research on iron sulfide scale, and this is due to some factors. One reason is as mentioned earlier that iron sulfide scale can present in many crystalline forms, and also in different iron to sulfur ratios, it is very sensitive to the conditions, and little variation in the condition can produce the formation of different form of iron sulfide deposition. In addition, iron sulfide solubility in water considered very low and it depend on the pH strongly. Another factor that makes iron sulfide scale is a challenge is that it is difficult to be studied in the laboratory compared to other conventional mineral scales, as maintaining the system oxygen-free is not an easy case in the laboratory experiments [41]. Such factors

have restricted the research and progress on iron sulfide scale formation, inhibition, removal, and prevention. However, more attention to iron sulfide scale is required in future work to overcome these challenges and produce more reliable output to resolve the iron sulfide scale issue in oil and gas wells.

Chapter 3: Theoretical Techniques

The Vienna Ab initio Simulation Package (VASP) version 5.4.4. code was used for all calculations [42], while Periodic Boundary Conditions (PBC) were applied for all the studied systems. The use of PBC enabled the approximation on a small scale based on the unit cell that represents the real large system. The reviewed Generalized Gradient Approximation of Perdew, Burke, and Ernzerhof (PBE-GGA), that provides superior equilibrium structural parameters compared to the Local Density Approximation (LDA) [43], [44] was applied for exchange-correlation energy for all components. For the explanation of the ion-electron interactions, the Projected Augmented Wave (PAW) pseudopotentials were included [45], [46]. Moreover, because of the significance of dispersion forces in labelling surfaces and interfaces, the semi-empirical correction by Grimme (DFT+D3) was involved in the calculation [47], [48]. The structure of the barite was obtained from the materials project database [49] and cleaved at the 001 surface. The 001 surface is known to be the most stable barite surface [24]. Both the 001 and 210 surfaces have the lowest surface energies. However, the former is the most stable unrelaxed surface [50] and hence used in this work. However, the 210 surface is calculated to be the most stable based on equilibrium morphology as opposed to the 001 surface, which is the most stable based on growth morphology. Nevertheless, the 001 is the most commonly observed surface [24], [51].

A supercell of 3 X 3 was created as the slab after cleaving with a vacuum region of 12 Å. The DFT calculations were based on the Gamma centered k-point sampling as this is computationally less expensive compared to the Monkhorst –Pack [52] while the plane wave cut-off energy was 530 eV. For the adsorption calculations, the inhibitors were placed

above the optimized slab surface of the barite The Quantum ATK virtual Nano lab [53], [54] was used for building the models, and materials studio [55] was used for visualization of results.

For the quantum chemical calculations of the optimized structures which was used in deducing the Quantitative Structure Activity Relationship (QSAR). Gaussian 09 [56] was employed and the three inhibitors were calculated at the B3LYP level of theory using the deftzvp basis set. These level of theory and basis set have been used in previous studies and known to give reliable result [19], [57]. All calculations were done in solvent implicitly using the polarizable continuum model-self-consistent reaction field (PCM-SCRF) [58].There were no imaginary frequencies ensuring that the molecules had reached a true minima.

Bulk configuration data obtained from the optimized system results. Table 3 shows the bulk configurations for the system of barite slab with 4 layers thickness, and the three inhibitors. Moreover, the axes (X, Y and Z) and unit cell volume are presented in Table 3.

Table 3. Bulk configuration for barite slab and the inhibitors in the system

SYSTEM	X (Å)	Y (Å)	Z (Å)	Unit cell volume ($Å^3$)
Barite Slab (4_Layers)	16.67	21.83	31	11280
DETPMP	34.13	26.27	30.17	27050
NTPM	27.28	26.24	25.9	18540
PASP	24.77	24.99	29.84	18480

A flow chart to describe the main steps of the theoretical techniques used to obtain the results of this project is presented in Figure 7.

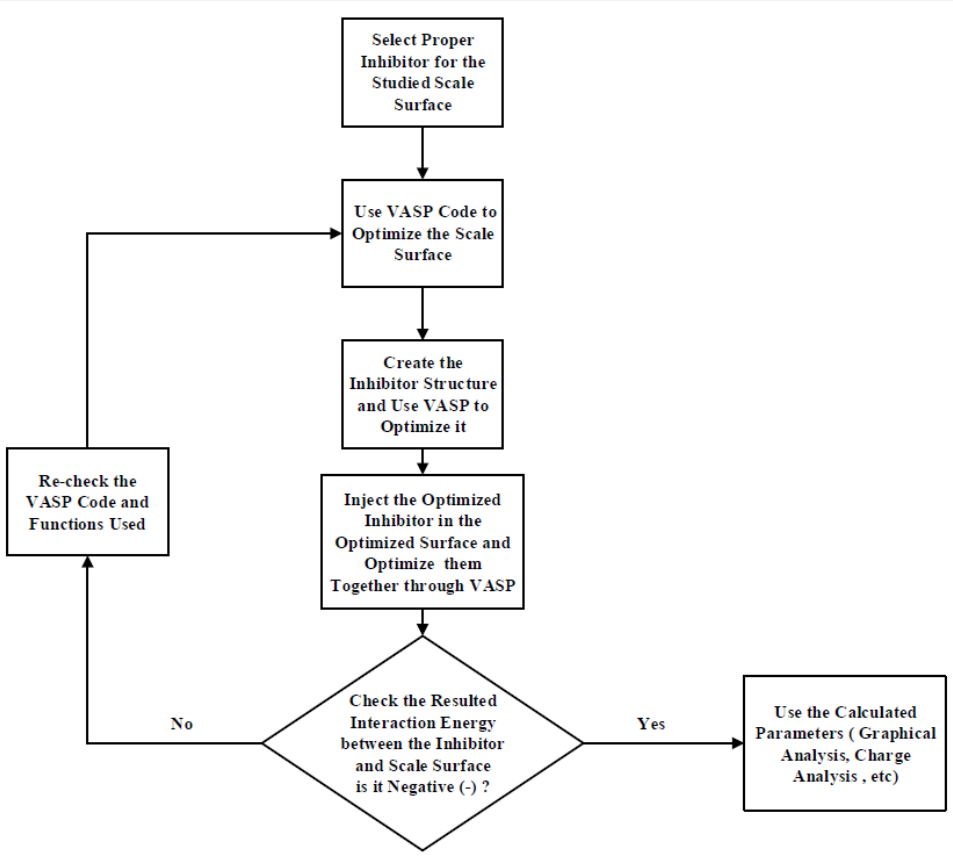

Figure 7. Flow chart for simulation program

In this work, scale inhibitors are theoretically studied using Density-Functional Theory (DFT) to understand the mechanisms of barite scale inhibition. The structures and properties of the three inhibitors (PASP, NTMP, and DETPMP) are presented in Figure 8 and Table 4, respectively. The compounds selected for studying the inhibition effect of barite scale are conventional inhibitors that are widely used for barite scale inhibition investigations [23]–[25]. Three different commercial inhibitors were selected for the simulation study to evaluate and compare their performance. Table 4 shows the main properties of the inhibitors used in this study, such as chemical name, formula, molecular

weight (Mw), and density. The density for inhibitors are obtained directly from Advanced Chemistry Development ACD/Labs Chemsketch software [26] , and the density values are at standard conditions (297.15 K, and 1 atm).

Table 4. Properties of Scale Inhibitors

Inhibitor	Chemical Name	Formula	Mw (Da*)	Density (g/cm^3)
PASP	Polyaspartic acid	$C_8H_{12}N_2O_7$	248.2	1.555±0.06
NTPM	Nitrilotrimethylenephosphonateand	$C_3H_{12}NO_9P_3$	299.1	2.094±0.06
DETPMP	Dimethylenetriaminepenta (methylene-phosphonic acid)	$C_9H_{28}N_3O_{15}P_5$	573.2	1.945±0.06

*1 Da is equivalent to 1 g/mol.

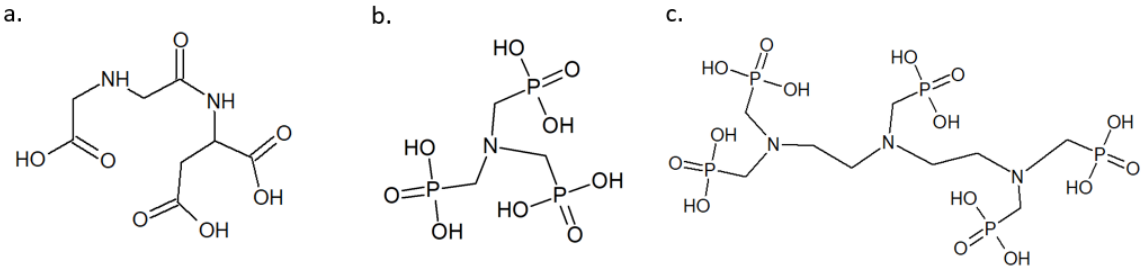

Figure 8. Structures of: (a) PASP, (b) NTPM, (c) DETPMP

Chapter 4: Results and Discussion

The interaction between the Barite slab surface and the three inhibitors was analyzed at two stages, by using two different thickness sizes or layers of the barite scale. The first part is the 4-layers barite slab surface, and the second part is the 2-layers barite slab surface. After that, the results of the two stages were compared and analyzed. Moreover, geometrical analysis, Quantitative Structure-Activity Relationship (QSAR) parameters calculation, and Eco-toxicity predictions were carried out to evaluate barite inhibition performance. Finally, the data for iron sulfide and calcite scales were presented and discussed.

4.1 4-Layers Barite Slab Surface

The molecular structure of each inhibitor was built and then optimized; the barite surface was simulated and optimized separately. Then, each optimized inhibitor was introduced into the optimized barite surface to study the interactions between the inhibitors molecules and the scale surface. Figure 9 shows the optimized 3-D structures for the inhibitors used in this study. From the structure of the three inhibitors, it is noticeable that DETPMP has the largest size compared to others, which can result in better inhibition properties.

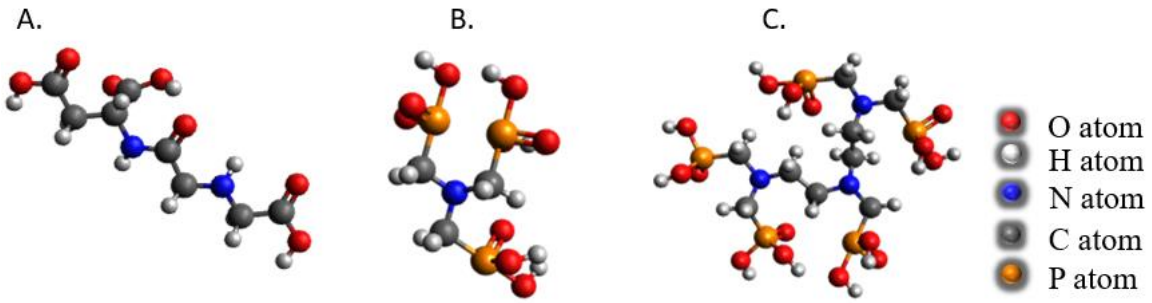

Figure 9. Optimized 3-D structures for the inhibitors: (A) PASP (B) NTPM, and (C) DETPMP

4.1.1 Interaction Energy Calculations

After building and optimizing the system of inhibitors and the barite ($BaSO_4$) scale, the interaction energy between the barite surface and the scale inhibitor molecules was calculated to evaluate the performance of the barite scale inhibitors' efficiency. The interaction energy is the total energy due to an interaction between the substances that are considered in the studied system. The interaction energy can be expressed as:

$$\Delta E = E_{(surface+inhibitor)} - \left(E_{surface} + E_{inhibitor}\right) \quad \text{Equation. (1)}$$

$E_{(surface+inhibitor)}$ is the energy of the optimized system with the inhibitor, $E_{surface}$is the optimized barite surface energy and it was fixed for all inhibitors since the same surface was used for the different inhibitors, and $E_{inhibitor}$ is the energy of the optimized inhibitor alone. Einhibitor is the energy of the optimized structure for each inhibitor. The inhibitor structure was generated by using Chemsketch software [26] , and optimized by using VASP simulation [42]. The values for $E_{inihbtor}$ for each inhibitor was obtained directly from the output data from the VASP simulation.

After optimizing the system, equation 1 was used to calculate the interaction energies for the three inhibitors; the results are summarized in Table 5.

Table 5. Interaction energies between the three inhibitors and the barite scale surface

Inhibitor	$E_{(surface+inhibitor)}$ (eV)	$E_{surface}$ (eV)	$E_{inhibitor}$ (eV)	ΔE (eV)
PASP	-2731.367	-2545.382	-184.927	-1.06
NTPM	-2712.668	-2545.382	-167.111	-0.17
DETPMP	-2903.677	-2545.382	-355.964	-2.33

The predicted interaction energies are all negative indicating the interaction between barite surface and the scale inhibitor. This interaction is expected to be spontaneous since all energy values are negative. The performance of the three inhibitors used in this study (PASP, NTPM, and DETPMP), can be classified as DETPMP >PASP>NTPM. DETPMP has resulted the highest negative value, hence it is obtained to show the highest binding with barite surface and the proposed order for the performance of the inhibitors is based on the calculated energies. Therefore, molecular simulations predicted that DETPMP to be more efficient in attracting the scale molecules compared to the other two inhibitors. This is likely due to the presence of more binding rings on DETPMP surface compared to other inhibitors. Moreover, a higher negative interaction energy value suggests the stability of the formed barite-inhibitor complex. These findings agrees with experimental findings that suggest DETPMP is a high efficiency scale inhibitor [25], [59].

4.1.2 Geometrical Analysis

The geometry of the optimized structure of the studied inhibitors on the barite slab was analyzed by considering four slab layers, the top three layers are relaxed, and the bottom layer fixed. Due to computational expenses and high number of atoms (up to 438 atom) on the system, this work utilizes four layers slab to conduct the calculation. Analysis of the geometry and 3-D figures of the optimized system can yield results of the bonds type that are formed, the number of bonds, and bond length between the surface and the scale inhibitors. Figure 10 demonstrates the optimized Barite surface slab alone and the complex of slab surface with the inhibitors.

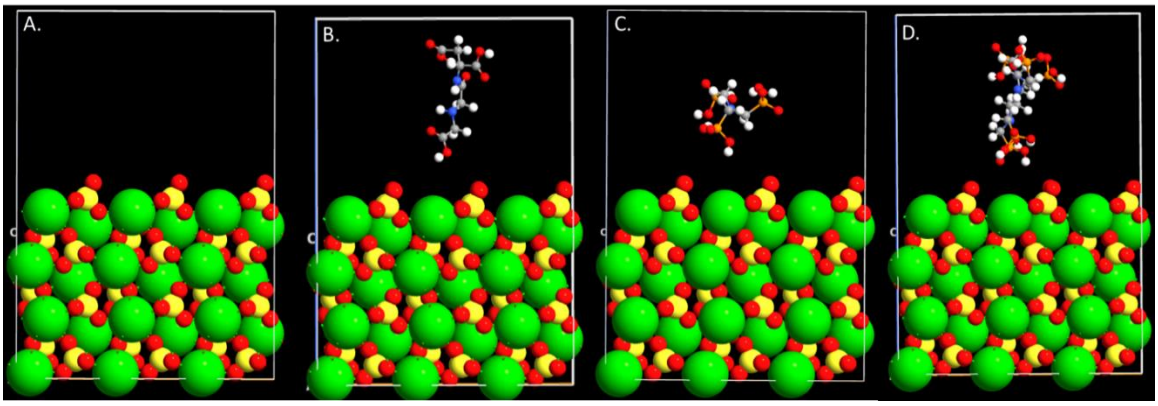

Figure 10. Optimized Structures of (A) Barite surface slab alone and with (B) PASP, (C) NTPM, and (D) DETPMP

Since the adsorption binding energy are relatively small for all the inhibitors, and the shortest distances calculated are higher than 3 Å for all inhibitors it proves that the mood of adsorption is physisorption rather than chemisorption [60]. It was observed that the physisorption connection could occur either through a Ba-O bond, that is the Ba atom from the barite slab surface and O atom from the scale inhibitor and an O-H bond, in which the O atom from the barite slab surface and H atom from the scale inhibitor. The calculated bonds distances are shown in Table 6, and, both the bond length and adsorption energies calculated confirms physisorption connection between the barite slab and inhibitors. Table 6 provides the predicted bond distances based on the O-H bond for each inhibitor with the barite slab. For PASP, NTPM, and DETPMP, example of the bond length calculated are 4.432 Å, 4.638 Å, and 3.346 Å, respectively. However, the shortest bond length found for DETPMP is 3.346 Å, and it means the interaction strength between the DETPMP inhibitor and the barite slab surface is higher compared to NTPM and PASP, which supports the previous findings from energy calculations and agree with experimental observations [25], [59].

Table 6. Calculated shortest bonds formed for each inhibitor

Inhibitor	bond (Å)
PASP	4.432
NTPM	4.638
DETPMP	3.346

Figure 11 illustrates the bond lengths formed between the barite slab surface and the inhibitors and the example bond length obtained in Table 6. From Figure 11 and Table 6 data, it is noticeable that DETPMP inhibitor is attracted more the barite slab surface (form shorter bond lengths), and this is obtained since it produced larger adsorption energy (4.1.1 section calculations).

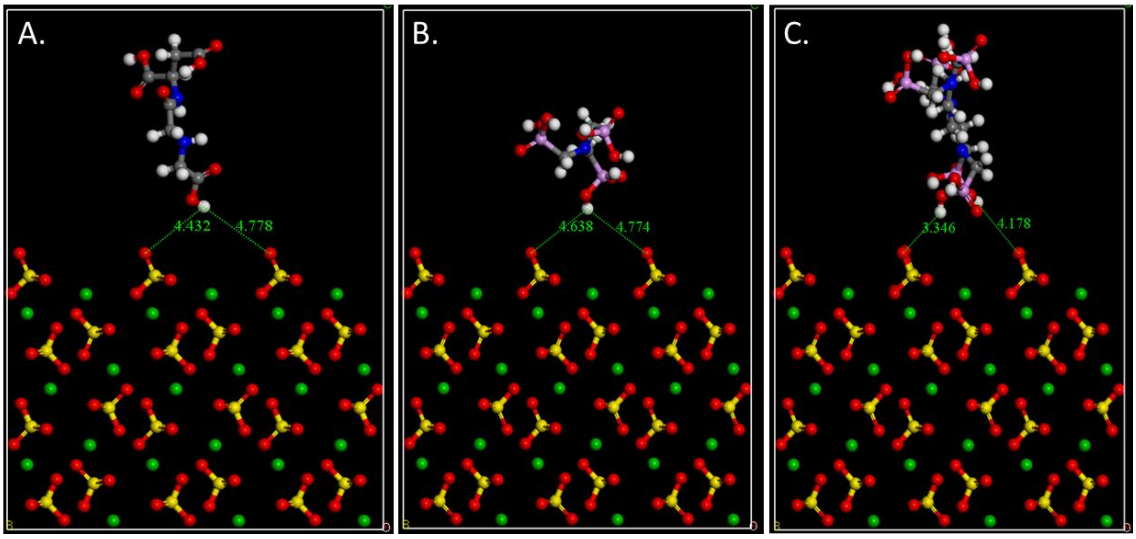

Figure 11. Bond lengths formed of the optimized structures of barite surface slab with (A) PASP, (B) NTPM, and (C) DETPMP

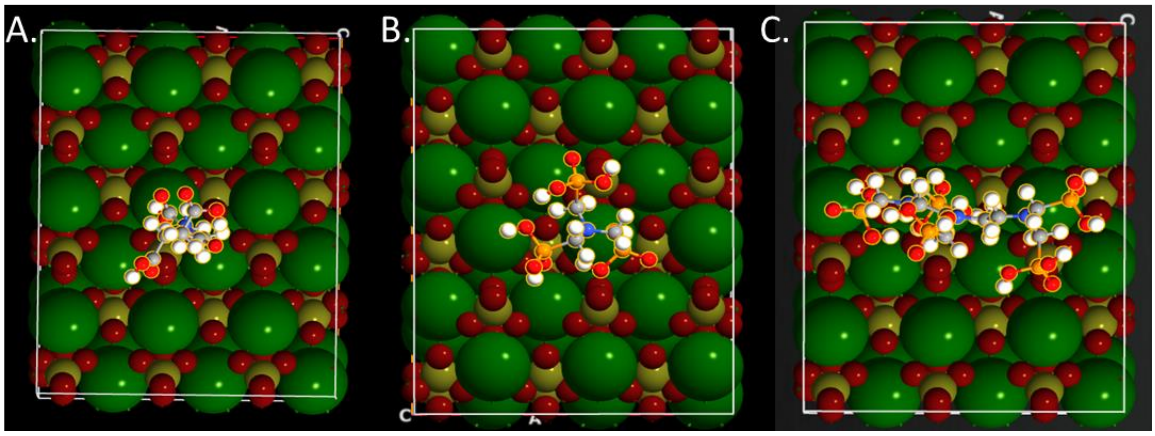

Figure 12. Top view for the barite slab with inhibitors: (A) PASP (B) NTPM, and (C) DETPMP

Addressing surface area aspect, it is observed as presented in Figure 12 that DETPMP covers more surface area compared to PASP and NTPM, and this is due to its large size. Figure 12 shows the top view of the barite surface with the three inhibitors after optimizing the system.

4.1.3 Charge Analysis

To further gain deeper insight into the mechanisms of interaction charge analysis was Bader charges [61], [62] relative to the valence electrons for each inhibitor (PASP, NTMP and DETPMP) before and after adsorption was computed. The charge densities of the three inhibitors (Fig. 3). However, the significant information is the charge difference before and after adsorption. For all the three inhibitors, the charge differences (Table S1, S2 and S3, in the appendix) are insignificant confirming that the mode of adsorption is physisorption. Nevertheless, it was observed that DETPMP had the largest charge difference which correlates with it having the highest adsorption energy. These charge differences occurs mostly on some of the phosphorus and oxygen atoms (Table S3) which suggests that the presence of these atoms in an inhibitor aids adsorption on barite scale. A similar

observation is noticed in the phosphorus atoms in NTMP but on a smaller scale compared to DETPMP as the former has fewer phosphorus atoms than the latter.

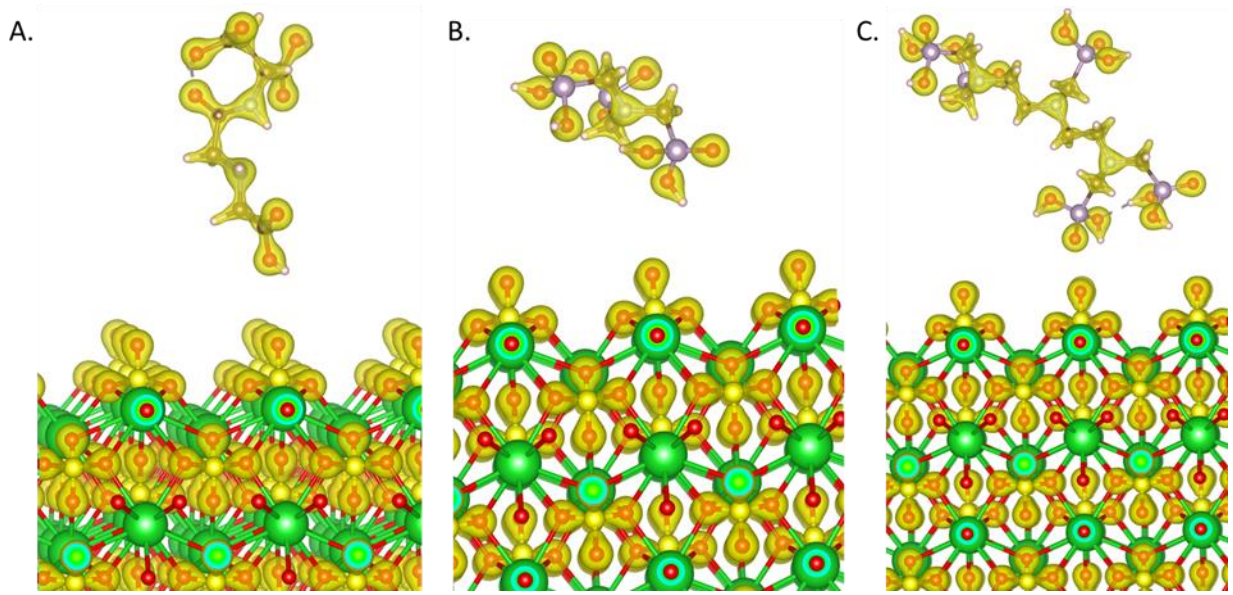

Figure 13. The charge densities of Barite surface slab with (A) PASP, (B) NTMP, and (C) DETPMP

4.1.4 QSAR Parameters Calculations

QSAR corresponds to the Quantitative Structure-Activity Relationship. This technique is used to predict the activity and reactivity of molecules on a system based on a set of equations and analyzing the resulted behavior. There are theoretical parameters that can be used to indicate the behavior of the inhibitors. Some of these parameters are (A) electron affinity (calculated by $A = -E_{LUMO}$) , (ΔN) amount of electron transfer, (I) ionization potential ($I = -E_{HOMO}$), (χ) electronegativity (calculated by $\chi = \frac{I+A}{2}$) , (η) global hardness (calculated by $\eta = \frac{I-A}{2}$) [63], [64]. (E_{HOMO}) Corresponds to the Energies of the Highest Occupied Molecular Orbital and (E_{LUMO}) corresponds to Energies of the Lowest

Unoccupied Molecular Orbital, and these two values can be obtained directly from the computational results. High (E_{HOMO}) values indicate good electron donation, and (E_{LUMO}) relates to the binding capability between the surface and inhibitor employing electron donating potential. If the difference between these two values $of\ E_{HOMO}\ and\ E_{HOMO}$ (ΔE_{L-H}) is small this means high adsorption occurs. Moreover, another critical parameter is calculated, which is the Total Negative Charge, (TNC); a high value of TNC indicates high adsorption of inhibitor molecule on the metal surface [65]. Table 7 summarizes the results of the calculated QSAR main parameters of the optimized system.

Table 7. QSAR parameters

COMPOUND	HOMO (eV)	LUMO (eV)	(ΔE_{L-H}) (eV)	I (eV)	A (eV)	η (eV)	χ (eV)	TNC (e)
PASP	-6.995	-0.786	6.210	6.995	0.786	3.105	3.891	-1.857
NTMP	-6.317	-0.091	6.225	6.317	0.091	3.113	3.204	-2.750
DETPMP	-6.100	-0.014	6.086	6.100	0.014	3.043	3.057	-4.599

The Ionization potential (I), which is calculated from $I = -E_{HOMO}$. The lower the ionization potential the higher the reactivity [65]. PASP has the highest ionization potential while DETPMP has the lowest ionization potential. This accounts for the high reactivity of DETPMP and explains its highest binding affinity with barite. On the other hand, the electronegativity (χ), which is calculated from $\chi = \frac{I+A}{2}$ [66], inhibitors with high electronegativity have lower reactivity and thus it has lower inhibition efficiency. Applying the same principle here yields that compound DETPMP has the lowest electronegativity value and hence it has better inhibition efficiency compared to other inhibitors studied.

Moreover, if the energy gap (ΔE_{L-H}) value is small it suggests high adsorption on the surface. Table 7 suggests that the energy gap was the lowest for inhibitor DETPMP and thus, it has the best adsorption potential and inhibition efficiency compared to PASP and NTPM on barite surface. In addition, TNC is another critical parameter that can describe the behavior of inhibitors in a system. Inhibitors with high TNC values can be considered having higher donation and adsorption electrons properties with the metal surface and these inhibitors show better inhibition effects. In this study, inhibitor DETPMP resulted the highest TNC followed by NTPM and PASP, respectively. Thus, according to the different QASR parameters, the order of inhibition efficiency for the studied inhibitors is DETPNP>NTPM>PASP.

4.1.4 Eco-Toxicity Predictions

ADMETSAR 2.0 software [67], [68] was employed to predict the eco-toxicological parameters of the studied inhibitors. To study the interaction of the inhibitors with the environment, the ecological toxicity (eco-tox) properties of the inhibitors were predicted to determine whether the studied inhibitors could be considered as environment-friendly molecules. The results of the predicted eco-tox properties are shown in Table 8. The three inhibitors resulted similar eco-tox properties. Moreover, all the inhibitors have been predicted to be safe with regard to Ames mutagenesis, biodegradation, crustacean aquatic toxicity, and fish aquatic toxicity. Looking at the carcinogenicity aspects, PASP is found to be safe, while NTPM and DETPMP were toxic. However, all the inhibitors could be toxic and slightly toxic with respect to eye irritation, acute oral toxicity (class III), and honey bee toxicity. Nevertheless, for acute oral toxicity, all inhibitors are slightly toxic, but it is not a critical parameter since these inhibitors are not expected to be consumed orally.

Moreover, for fish aquatic toxicity, all inhibitors were safe, which suggests that they would not raise problems even if they were used for offshore production operations.

For solubility in water, the three compounds resulted similar behavior ranging from very soluble to highly soluble. Moreover, the water solubility of the inhibitors can be referred to through the presence of hydroxyl OH groups in all inhibitors and as the number of OH groups increase the solubility increases. DETPMP has the highest number of OH groups, hence it has the highest water solubility compared to other inhibitors, and this was confirmed by the eco-tox predications in Table 8. The simulation predictions for solubility are compared to the reported properties in their product data sheet [69] and they are in agreement that suggest all three inhibitors are soluble in water.

Table 8 shows that all inhibitors have similar eco-tox properties. Moreover, the previous calculations from QSAR parameters have shown a trend that supports the findings that DETPMP inhibitor has the highest inhibition efficiency. In addition, the interaction energy calculation and geometry analysis both support the same conclusions. Furthermore, an experimental study has analyzed the mechanism of barium sulfate deposition inhibition for multi-scale inhibitors [25]. This experimental study on barite scale inhibition indicated that DETPMP inhibitor has a very high efficiency compared to other classical inhibitors such as PPCA (phosphinopoly carboxylic acid), and SPCA (sulfonated poly(carboxylic acid)), which supports the conclusions of this theoretical investigation [25].

Table 8. Predicted eco-toxicity properties of the studied inhibitors

		PASP	NTMP	DETPMP
S/N	CATEGORY	PROBABILITY (REMARK)	PROBABILITY (REMARK)	PROBABILITY (REMARK)
1	Carcinogenicity	(Safe) 0.76	(Toxic) 0.63	(Toxic) 0.63
2	Eye irritation	(Slightly toxic) 0.64	(Toxic) 0.96	(Toxic) 0.81
3	Ames mutagenesis	(Safe) 0.61	(Safe) 0.76	(Safe) 0.68
4	Acute Oral Toxicity (class III)	(Slightly toxic) 0.82	(Slightly toxic) 0.67	(Slightly toxic) 0.74
5	Honey bee toxicity	(Slightly dangerous) 0.53	(Slightly toxic) 0.57	(Slightly toxic) 0.57
6	Biodegradation	(Safe) 0.65	(Safe) 0.68	(Safe) 0.63
7	Crustacean aquatic toxicity	(Safe) 0.91	(Safe) 0.87	(Safe) 0.67
8	Fish aquatic toxicity	(Safe) 0.56	(Safe) 0.92	(Safe) 0.84
9	Water solubility (log S)	(Very soluble) -0.85	(Very soluble) -0.20	(Highly Soluble) -1.01

DETPMP is a classical inhibitor that used a lot for scale inhibition, and it is experimentally proven that it has an excellent performance in inhibiting barite scale [27], [70], [71]. Moreover, the theoretical studies provide insights into why DETPMP has a superior performance compared to the other two inhibitors, PASP and NTMP. DETMP has the highest adsorption energy, moreover the optimized structure of the inhibitors on the barite scale slab shows that DETPMP has covers a large surface area on the scale compared to

the other two inhibitors. Furthermore, the QSAR studies show that the structure of DETPMP contributes to its activity in being a good inhibitor of superior performance by having the lowest ionization energy, nucleophilicity, and electronegativity and the smallest band gap and highest total negative charge. All of which correlates to the characteristics of a compound that can serve as a good inhibitor.

4.2 2-Layers Slab Barite Surface

After obtaining the data from 4 layers thickness barite slab, a sensitivity analysis was done by decreasing the number of slabs to two layers to check the adsorption energy calculation. Decreasing the number of barite layers means less barite thickness in real scenarios. The adsorption energies calculation for two layers barite slab are summarized in Table 9.

Table 9. Interaction energies between the three inhibitors and the barite scale surface for two layers barite slab

Inhibitor	$E_{(surface+inhibitor)}$ (eV)	$E_{surface}$ (eV)	$E_{inhibitor}$ (eV)	ΔE_{ads} (eV)
PASP	-1626.340	-1441.392	-184.927	-0.02
NTPM	-1608.540	-1441.392	-167.111	-0.04
DETPMP	-1797.487	-1441.392	-355.964	-0.13

Figure 14 displays the calculated adsorption energies for both thickness surfaces. It's observed that the four-layers barite slab yield higher adsorption energies for all the three inhibitors, and it means it's more realistic comparing to the two-layers slab surface. Moreover, the 4-layers slab barite surface produced higher adsorption energy for all the

inhibitors than the 2-layers slab barite surface, which suggests for more amount of the scale surface, produce higher interaction between the scale surface and the scale inhibitor.

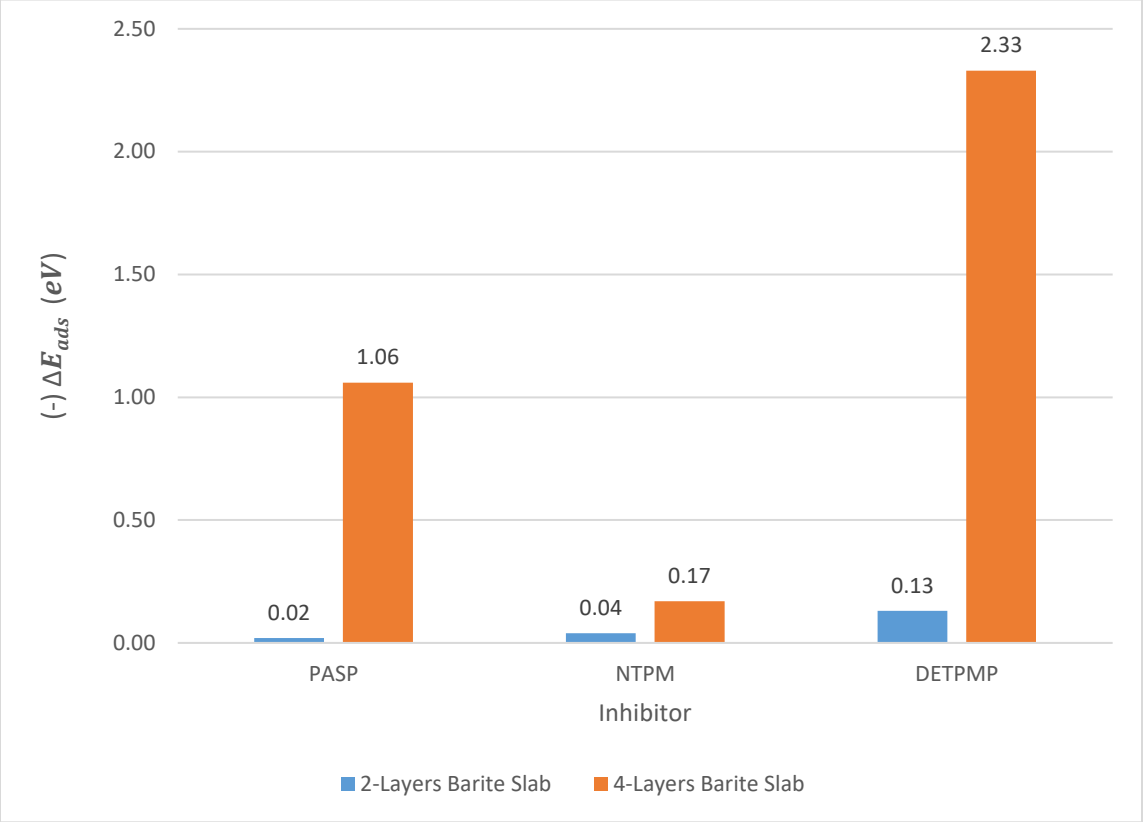

Figure 14. Comparing adsorption energies for 2-layers slab and 4-layers slab of barite surface

The optimized structures for the two-layer slab surface and the three inhibitors injected on the system are presented in Figure 15.

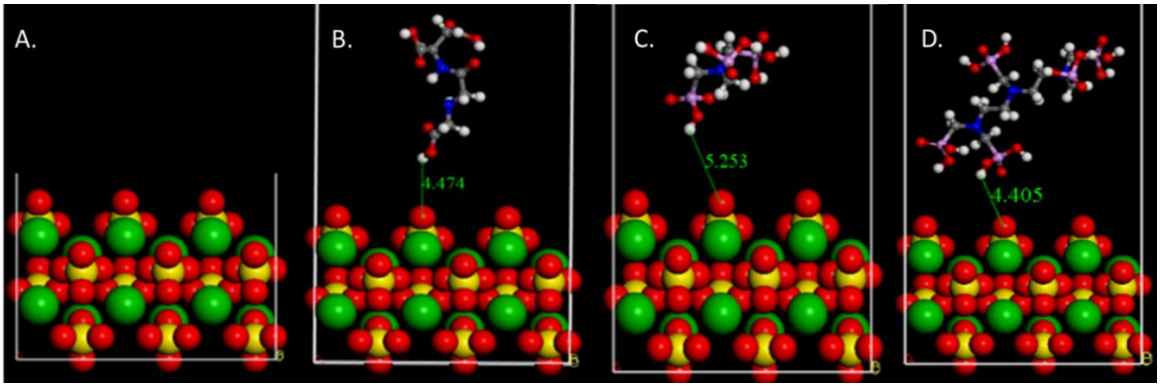

Figure 15. 2-layers slab optimized Structures of (A) Barite surface slab alone and with (B) PASP, (C) NTPM, and (D) DETPMP

Table 10 provides the predicted bond distances based on the shortest O-H bond for each inhibitor with the barite slab. The data for the bond formed are calculated from the optimized system based on the closest two atoms to each other that could form a bond between the surface and the scale inhibitors. For PASP, NTPM, and DETPMP, the shortest predicted bond formed is 4.474 Å, 5.253 Å, and 4.405 Å, respectively.

Table 10. Bond lengths for 2-layers barite slab surface

Inhibitor	Shortest bond (Å)
PASP	4.474
NTPM	5.253
DETPMP	4.405

Again, even for the 2-layers slab surface the predicted values for bond lengths are higher than 3 Å, and hence, it suggests physisorption connection between the scale surface and the inhibitors.

4.3 Iron Sulfide and Calcite Inhibition Calculations

For iron sulfide and calcite inhibition calculation, Polyepoxysuccinic Acid (PESA), Hydrolyzed Polymaleic Anhydride (HPMA) and Polyaspartic Acid (PASP) classical inhibitors were used. Figure16 illustrates the 2-strcutre of these inhibitors, and Figure 17 illustrate the optimized 3-D Figures of the inhibitors.

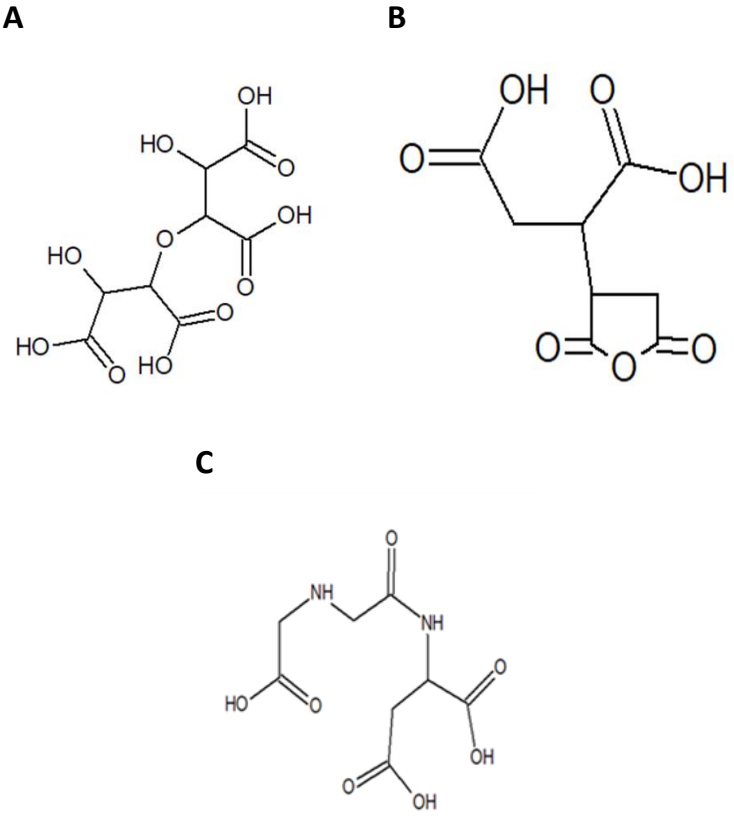

Figure 16. 2-D structure of (A) PESA, (B) HPMA, (C) PASP

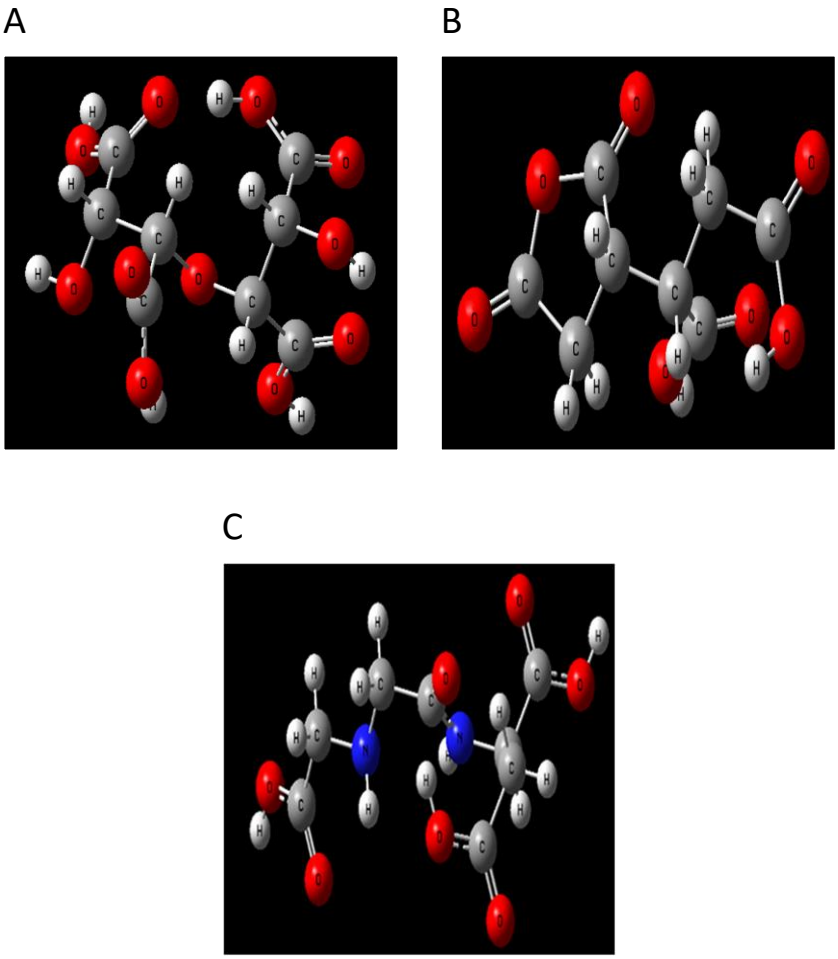

Figure 17. Optimized 3-D structure of (A) PESA, (B) HPMA, (C) PASP

The calculated data for iron sulfide and calcite scale surfaces are shown in Table 11.

Table 11. Adsorption energies for iron sulfide surface and calcite surface

	Inhibitor	$E_{(surface+inhibitor)}$ (eV)	$E_{surface}$ (eV)	$E_{inhibitor}$ (eV)	ΔE (eV)
Iron Sulfide Surface	Fe_PESA	-2400.385	-1263.580	-1138.721	1.916
	Fe_HPMA	-2099.083	-1263.580	-836.533	1.030
	Fe_PASP	-2210.603	-1263.580	-2545.382	1.43
Calcite Surface	Ca_PESA	-1814.425	-677.466	-1138.721	1.761
	Ca_HPMA	-1513.158	-677.466	-836.533	0.841
	Ca_PASP	-1624.638	-677.466	-948.458	1.287

It is clear from Table 11 that the adsorption energies are positive for all inhibitors and both scale surfaces. In addition, this suggests there are no attraction or binding between the inhibitor and the scale surface, which means no inhibition process might occur. However, the used inhibitors are classical inhibitors for iron sulfide and calcite scales, so the binding energy results should be negative. These data are obtained from the preliminary simulation model. After analyzing the model used for these calculations, some modifications were applied to the simulation model to generate better data that match with experimental studies and findings. Therefore, after developing the model a better data obtained.

Chapter 5: Conclusions

Scale formation phenomena is a severe problem in oil and gas production wells, especially the barite scale. During oil and gas production, the scale deposition occurs in many forms and shapes, it can precipitate along the entire process tubes, and causes blocking flow leading to production and economic losses. Understanding the inhibition mechanism of classical inhibitor is expected to facilitate the design of new inhibitors to improve performance economics and environmental impact. In this paper, the performance and eco-toxicity of three different barite scale inhibitors (PASP, NTPM, and DETPMP) have been evaluated using molecular simulation tools. The interaction energies between the barite surface and the scale inhibitors have suggested the following order of inhibitor strength as DETPMP>PASP> NTPM. Furthermore, the geometrical analysis of the system and scale inhibitors supported the same sequence of inhibition strength as DETPMP>PASP>NTPM. Moreover, the investigation of QSAR parameters such as TNC verified that DETPMP has the highest inhibition efficiency in comparison with other inhibitors. Besides, all inhibitors have shown similar eco-tox properties. A sensitivity analysis was carried out to compare the thickness of the barite slab surface and its effect on the adsorption energy calculation, it yields that the 4-layers surface barite slab used results are more accurate and realistic. This study reveals the agreement of theoretical and experimental findings and indicates that molecular simulation tools can be used to screen and predict the performance of scale inhibitors and even design new green inhibitor compounds. Future work will focus on using these theoretical techniques to generate more environmental and green scale inhibitors with high efficiency compared to the classical inhibitors used nowadays.

References

[1] M. S. Kamal, I. Hussein, M. Mahmoud, A. S. Sultan, and M. A. S. Saad, “Oilfield scale formation and chemical removal: A review,” *J. Pet. Sci. Eng.*, vol. 171, no. July, pp. 127–139, 2018.

[2] M. M. Jordan, H. Williams, S. Linares-Samaniego, and D. M. Frigo, “New insights on the impact of high temperature conditions (176°C) on carbonate and sulphate scale dissolver performance,” *Soc. Pet. Eng. - SPE Int. Conf. Exhib. Oilf. Scale 2014*, pp. 495–511, 2014.

[3] K. Sawada, “The mechanisms of crystallization and transformation of calcium carbonates,” *Pure Appl. Chem.*, vol. 69, no. 5, pp. 921–928, 1997.

[4] J. Li, M. Tang, Z. Ye, L. Chen, and Y. Zhou, “Scale formation and control in oil and gas fields: A review,” *Journal of Dispersion Science and Technology*. 2017.

[5] W. Y. Shi *et al.*, “Molecular dynamics simulation for interaction of PESA and acrylic copolymers with calcite crystal surfaces,” *Desalination*, vol. 291, pp. 8–14, 2012.

[6] A. Yuchi, Y. Gotoh, and S. Itoh, “Potentiometry of effective concentration of polyacrylate as scale inhibitor,” *Anal. Chim. Acta*, vol. 594, no. 2, pp. 199–203, 2007.

[7] A. Haghtalab, M. J. Kamali, and A. Shahrabadi, “Prediction mineral scale formation in oil reservoirs during water injection,” *Fluid Phase Equilib.*, vol. 373, pp. 43–54, 2014.

[8] A. A. Olajire, “A review of oilfield scale management technology for oil and gas production,” *J. Pet. Sci. Eng.*, vol. 135, pp. 723–737, 2015.

[9] T. Chen, Q. Wang, F. Chang, and N. Aljeaban, “Recent development and remaining challenges of iron sulfide scale mitigation in sour gas wells,” *Int. Pet. Technol. Conf. 2019, IPTC 2019*, no. March, pp. 26–28, 2019.

[10] Q. Wang *et al.*, “Iron sulfide and removal in scale formation sour gas wells,” *Soc. Pet. Eng. - SPE Int. Oilf. Scale Conf. Exhib.*, 2016.

[11] L. Sanders, X. Hu, E. Mavredaki, V. Eroini, R. Barker, and A. Neville, “Assessment of combined scale/corrosion inhibitors - A combined jar test/bubble cell,” *J. Pet. Sci. Eng.*, vol. 118, pp. 126–139, 2014.

[12] S. Lee and C. H. Lee, “Effect of operating conditions on CaSO4 scale formation mechanism in nanofiltration for water softening,” *Water Res.*, vol. 34, no. 15, pp. 3854–3866, 2000.

[13] M. S. Kamal, I. Hussein, M. Mahmoud, A. S. Sultan, and M. A. S. Saad, “Oilfield scale formation and chemical removal: A review,” *J. Pet. Sci. Eng.*, vol. 171, no. January, pp. 127–139, 2018.

[14] S. Kumar, T. K. Naiya, and T. Kumar, “Developments in oilfield scale handling towards green technology-A review,” *J. Pet. Sci. Eng.*, vol. 169, pp. 428–444, 2018.

[15] E. Oddo, M. B. Tomson, and U. Rice, “Why Scale Forms and How To Predict It,” no. February, pp. 47–54, 1994.

[16] H. A. Nasr-El-Din, A. Y. Al-Humaidan, S. K. Mohamed, and A. M. Al-Salman,

"Iron Sulfide Formation in Water Supply Wells With Gas Lift," *Proc. - SPE Int. Symp. Oilf. Chem.*, pp. 425–440, 2001.

[17] P. Risthaus, D. Bosbach, U. Becker, and A. Putnis, "Barite scale formation and dissolution at high ionic strength studied with atomic force microscopy," *Colloids Surfaces A Physicochem. Eng. Asp.*, vol. 191, no. 3, pp. 201–214, 2001.

[18] M. Ahmed, A. Onawole, I. Hussien, M. Saad, M. Mahmoud, and H. Nimir, "Effect of pH on Dissolution of Iron Sulfide Scales Using THPS," in *SPE International Conference on Oilfield Chemistry, 8-9 April, Galveston, Texas, USA*, 2019, pp. 1–9.

[19] A. T. Onawole, I. A. Hussein, M. A. Saad, M. Mahmoud, M. E. M. Ahmed, and H. I. Nimir, "Effect of pH on acidic and basic chelating agents used in the removal of iron sulfide scales: A computational study," *J. Pet. Sci. Eng.*, vol. 178, pp. 649–654, 2019.

[20] C. Ruiz-Agudo, C. V. Putnis, E. Ruiz-Agudo, and A. Putnis, "The influence of pH on barite nucleation and growth," *Chem. Geol.*, vol. 391, pp. 7–18, 2015.

[21] S. S. Shaw and K. S. Sorbie, "The effect of pH on static barium sulphate inhibition efficiency and minimum inhibitor concentration of generic scale inhibitors," *Soc. Pet. Eng. - SPE Int. Conf. Exhib. Oilf. Scale 2012*, vol. 5, no. Figure 5, pp. 247–264, 2012.

[22] B. S. Bageri, M. A. Mahmoud, R. A. Shawabkeh, S. H. Al-Mutairi, and A. Abdulraheem, "Toward a Complete Removal of Barite (Barium Sulfate BaSO 4) Scale Using Chelating Agents and Catalysts," *Arab. J. Sci. Eng.*, vol. 42, no. 4, pp.

1667–1674, 2017.

[23] C. Li, C. Zhang, and W. Zhang, “The inhibition effect mechanisms of four scale inhibitors on the formation and crystal growth of CaCO3 in solution,” *Sci. Rep.*, vol. 9, no. 1, pp. 1–11, 2019.

[24] F. Jones, W. R. Richmond, and A. L. Rohl, “Molecular modeling of phosphonate molecules onto barium sulfate terraced surfaces,” *J. Phys. Chem. B*, 2006.

[25] A. Y. T. Lu *et al.*, “The Mechanism of Barium Sulfate Deposition Inhibition and the Prediction of Inhibitor Dosage,” *J. Chem. Eng. Data*, vol. 64, no. 11, pp. 4968–4976, 2019.

[26] ACD/Labs, “Advanced Chemistry Development (ACD/Labs) Software,” 2005. [Online]. Available: ACD/ChemSketch, version 2019.1.3, Advanced Chemistry Development, Inc., Toronto, ON, Canada, www.acdlabs.com, 2020.

[27] A. T. Kan, G. Fu, M. B. Tomson, M. Al-Thubaiti, and A. J. Xiao, “Factors affecting scale inhibitor retention in carbonate-rich formation during squeeze treatment,” *SPE J.*, vol. 9, no. 3, pp. 280–289, 2004.

[28] B. G. Al-Harbi, A. J. Graham, and K. S. Sorbie, “Iron Sulfide Inhibition and Interaction With Zinc and Lead Sulfides,” *SPE Prod. Oper.*, no. April, pp. 20–21, 2018.

[29] N. Bhandari, M. Bhandari, I. Littlehales, and J. Fidoe, “Development of a novel iron sulfide scale inhibitor for onshore US application,” *Proc. - SPE Int. Symp. Oilf. Chem.*, vol. 2019, 2019.

[30] M. M. Vazirian, T. T. J. Charpentier, A. Neville, F. B. Alvim, and M. De Oliveira Penna, “Assessing surface engineering solutions for oilfield scale; correlating laboratory tests to field trials,” *Soc. Pet. Eng. - SPE Int. Oilf. Scale Conf. Exhib.*, pp. 1–14, 2016.

[31] G. Verri *et al.*, “Iron sulfide scale management in High-H2S and -CO2 carbonate reservoirs,” *SPE Prod. Oper.*, vol. 32, no. 3, pp. 305–313, 2017.

[32] M. Alahmad, “Factors affecting scale formation in sea water environments - An experimental approach,” *Chem. Eng. Technol.*, vol. 31, no. 1, pp. 149–156, 2008.

[33] J. J. Wylde, “Sulfide scale control in produced water handling and injection systems: Best practices and global experience overview,” *Soc. Pet. Eng. - SPE Int. Conf. Exhib. Oilf. Scale 2014*, pp. 366–380, 2014.

[34] Q. Wang, T. Chen, F. Chang, W. Al-Nasser, and F. Liang, “Searching for iron sulfide scale dissolver for downhole applications,” *NACE - Int. Corros. Conf. Ser.*, vol. 2018-April, no. 10545, pp. 1–10, 2018.

[35] Z. Liu, Y. Sun, X. Zhou, T. Wu, Y. Tian, and Y. Wang, “Synthesis and scale inhibitor performance of polyaspartic acid,” *J. Environ. Sci.*, vol. 23, no. SUPPL., pp. S153–S155, 2011.

[36] S. Elkatatny, “New formulation for iron sulfide scale removal,” *SPE Middle East Oil Gas Show Conf. MEOS, Proc.*, vol. 2017-March, no. March, pp. 1809–1821, 2017.

[37] T. Chen, H. Montgomerie, P. Chen, T. Hagen, and S. Kegg, “Development of

environmental friendly iron sulfide inhibitors for field application," *Proc. - SPE Int. Symp. Oilf. Chem.*, vol. 1, pp. 259–268, 2009.

[38] T. Almubarak, J. H. Ng, and H. Nasr-El-Din, "Chelating agents in productivity enhancement: A review," *Soc. Pet. Eng. - SPE Oklahoma City Oil Gas Symp. 2017*, no. March, pp. 88–112, 2017.

[39] B. S. Bageri, M. A. Mahmoud, R. A. Shawabkeh, S. H. Al-Mutairi, and A. Abdulraheem, "Toward a Complete Removal of Barite (Barium Sulfate BaSO4) Scale Using Chelating Agents and Catalysts," *Arab. J. Sci. Eng.*, vol. 42, no. 4, pp. 1667–1674, 2017.

[40] A. S. Metcalf, C. P. Parker, and J. L. Boles, "Acetic acid demonstrates greater carbonate dissolution than typically expected," *Can. Int. Pet. Conf. 2004, CIPC 2004*, no. 1, pp. 2–4, 2004.

[41] T. Chen, Q. Wang, F. Chang, and N. Aljeaban, "Recent development and remaining challenges of iron sulfide scale mitigation in sour gas wells," *Int. Pet. Technol. Conf. 2019, IPTC 2019*, pp. 1–11, 2019.

[42] G. Kresse and D. Joubert, "From ultrasoft pseudopotentials to the projector augmented-wave method," *Phys. Rev. B*, vol. 59, no. 3, pp. 1758–1775, Jan. 1999.

[43] L. M. Yang, E. Ganz, S. Svelle, and M. Tilset, "Computational exploration of newly synthesized zirconium metal-organic frameworks UiO-66, -67, -68 and analogues," *J. Mater. Chem. C*, 2014.

[44] J. P. Perdew, K. Burke, and M. Ernzerhof, "Generalized gradient approximation

made simple," *Phys. Rev. Lett.*, 1996.

[45] H. Toulhoat, P. Raybaud, S. Kasztelan, G. Kresse, and J. Hafner, "Transition metals to sulfur binding energies relationship to catalytic activities in HDS: Back to Sabatier with first principle calculations," *Catal. Today*, 1999.

[46] P. E. Blöchl, "Generalized separable potentials for electronic-structure calculations," *Phys. Rev. B*, 1990.

[47] J. B. A. Davis, F. Baletto, and R. L. Johnston, "The Effect of Dispersion Correction on the Adsorption of CO on Metallic Nanoparticles," *J. Phys. Chem. A*, 2015.

[48] S. Grimme, J. Antony, S. Ehrlich, and H. Krieg, "A consistent and accurate ab initio parametrization of density functional dispersion correction (DFT-D) for the 94 elements H-Pu," *J. Chem. Phys.*, 2010.

[49] K. Persson, "Materials Data on BaSO4 (SG:62) by Materials Project." United States, 2014.

[50] N. L. Allan, A. L. Rohl, D. H. Gay, C. R. A. Catlow, R. J. Davey, and W. C. MacKrodt, "Calculated bulk and surface properties of sulfates," *Faraday Discuss.*, vol. 95, pp. 273–280, 1993.

[51] F. Jones and A. L. Rohl, "Using Molecular Modelling to Understand and Predict the Impact of Organic Additives as Crystal Growth Modifiers," *Aust. J. Chem.*, pp. 724–733, 2019.

[52] P. Kratzer and J. Neugebauer, "The basics of electronic structure theory for periodic systems," *Front. Chem.*, vol. 7, no. MAR, pp. 1–18, 2019.

[53] S. Smidstrup *et al.*, “QuantumATK: An integrated platform of electronic and atomic-scale modelling tools,” *J. Phys. Condens. Matter*, 2020.

[54] A. T. Onawole, I. A. Hussein, M. E. M. Ahmed, M. A. Saad, and S. Aparicio, “Ab Initio molecular dynamics of the dissolution of oilfield pyrite scale using borax,” *J. Mol. Liq.*, 2020.

[55] Dassault Systèmes, “BIOVIA Materials Studio.” San Diego:, 2017.

[56] M. J. Frisch *et al.*, “Gaussian 09, Revision D.01,” *Gaussian, Inc. Wallingford CT*. Gaussian, Inc. TS - CrossRef Metadata Search, Wallingford CT, 2013.

[57] A. T. Onawole, I. A. Hussein, A. Sultan, S. Abdel-Azeim, M. Mahmoud, and M. A. Saad, “Molecular and electronic structure elucidation of Fe 2+ /Fe 3+ complexed chelators used in iron sulphide scale removal in oil and gas wells,” *Can. J. Chem. Eng.*, vol. 97, no. 7, pp. 2021–2027, 2019.

[58] J. Tomasi, B. Mennucci, and R. Cammi, “Quantum mechanical continuum solvation models,” *Chem. Rev*, no. 105, pp. 2999–3093, 2005.

[59] K. Jarrahian, M. Singleton, L. Boak, and K. S. Sorbie, “Surface Chemistry of Phosphonate Scale Inhibitor Retention Mechanisms in Carbonate Reservoirs,” 2020.

[60] A. Hamza, I. A. Hussein, M. J. Al-Marri, M. Mahmoud, R. Shawabkeh, and S. Aparicio, “CO2 enhanced gas recovery and sequestration in depleted gas reservoirs: A review,” *J. Pet. Sci. Eng.*, vol. 196, p. 107685, 2021.

[61] R. F. W. Bader, “Atoms in molecules,” *Acc. Chem. Res.*, vol. 18, no. 1, pp. 9–15, 1985.

[62] G. Henkelman, A. Arnaldsson, and H. Jónsson, “A fast and robust algorithm for Bader decomposition of charge density,” *Comput. Mater. Sci.*, vol. 36, no. 3, pp. 354–360, Jun. 2006.

[63] E. E. Ebenso *et al.*, “Quantum chemical investigations on quinoline derivatives as effective corrosion inhibitors for mild steel in acidic medium,” *Int. J. Electrochem. Sci.*, vol. 7, no. 6, pp. 5643–5676, 2012.

[64] Z. El Adnani *et al.*, “DFT Study of 7-R-3methylquinoxalin-2(1H)-ones (R=H; CH 3 ; Cl) as Corrosion Inhibitors in Hydrochloric Acid,” *Int. J. Electrochem. Sci.*, vol. 7, Aug. 2012.

[65] K. O. Sulaiman and A. T. Onawole, “Quantum chemical evaluation of the corrosion inhibition of novel aromatic hydrazide derivatives on mild steel in hydrochloric acid,” *Comput. Theor. Chem.*, vol. 1093, pp. 73–80, 2016.

[66] K. O. Sulaiman and A. T. Onawole, “Quantum chemical evaluation of the corrosion inhibition of novel aromatic hydrazide derivatives on mild steel in hydrochloric acid,” *Comput. Theor. Chem.*, vol. 1093, pp. 73–80, 2016.

[67] H. Yang *et al.*, “admetSAR 2.0: web-service for prediction and optimization of chemical ADMET properties,” *Bioinformatics*, vol. 35, no. 6, pp. 1067–1069, Aug. 2019.

[68] H. Yang, L. Sun, Z. Wang, W. Li, G. Liu, and Y. Tang, “ADMETopt: A Web Server for ADMET Optimization in Drug Design via Scaffold Hopping,” *J. Chem. Inf. Model.*, vol. 58, no. 10, pp. 2051–2056, Oct. 2018.

[69] “MSDS.” [Online]. Available: https://www.msdsonline.com/sds-search/.

[70] A. R. Golsefatan, M. Safari, and M. Jamialahmadi, “Using silica nanoparticles to improve DETPMP scale inhibitor performance as a novel calcium sulfate inhibitor,” *Desalin. Water Treat.*, vol. 57, no. 44, pp. 20800–20808, 2016.

[71] G. M. Graham, L. S. Boak, and C. M. Hobden, “Examination of the effect of generically different scale inhibitor species (PPCA and DETPMP) on the adherence and growth of barium sulphate scale on metal surfaces,” *Soc. Pet. Eng. - Int. Symp. Oilf. Scale 2001*, 2001.

Appendix

Table S1. The valence Bader charges of PASP before and after adsorption on Barite

#	Element	Before Adsorption	After adsorption	Charge Difference
1	Carbon	2.451	2.475	0.024
2	Carbon	3.637	3.751	0.114
3	Carbon	3.742	3.761	0.019
4	Carbon	2.585	2.607	0.022
5	Carbon	3.683	3.617	-0.066
6	Carbon	2.457	2.509	0.051
7	Carbon	4.031	4.044	0.013
8	Carbon	2.514	2.483	-0.031
9	Hydrogen	0.328	0.332	0.004
10	Hydrogen	0.951	0.887	-0.064
11	Hydrogen	0.943	0.940	-0.004
12	Hydrogen	0.547	0.599	0.052
13	Hydrogen	0.937	0.928	-0.010
14	Hydrogen	0.947	0.898	-0.049
15	Hydrogen	0.541	0.485	-0.056
16	Hydrogen	0.898	0.917	0.020
17	Hydrogen	0.362	0.348	-0.015
18	Hydrogen	0.943	0.898	-0.045
19	Hydrogen	0.896	0.899	0.003
20	Hydrogen	0.341	0.301	-0.040
21	Nitrogen	6.123	6.028	-0.095
22	Nitrogen	6.146	6.243	0.096
23	Oxygen	7.163	7.129	-0.035
24	Oxygen	7.165	7.149	-0.017
25	Oxygen	7.155	7.158	0.003

26	Oxygen	7.117	7.116	-0.001
27	Oxygen	7.158	7.156	-0.001
28	Oxygen	7.123	7.159	0.037
29	Oxygen	7.114	7.184	0.069
	Total	96.000	95.999	

Table S2. The valence Bader charges of NTMP before and after adsorption on Barite

S/N	Element	Before Adsorption	After adsorption	Charge Difference
1	Carbon	4.186	4.099	-0.087
2	Carbon	4.093	4.127	0.034
3	Carbon	4.128	4.138	0.010
4	Hydrogen	0.900	0.920	0.021
5	Hydrogen	0.921	0.916	-0.006
6	Hydrogen	0.901	0.880	-0.021
7	Hydrogen	0.894	0.908	0.014
8	Hydrogen	0.850	0.852	0.002
9	Hydrogen	0.907	0.922	0.015
10	Hydrogen	0.316	0.322	0.006
11	Hydrogen	0.338	0.342	0.004
12	Hydrogen	0.294	0.306	0.012
13	Hydrogen	0.299	0.321	0.022
14	Hydrogen	0.303	0.306	0.003
15	Hydrogen	0.341	0.218	-0.123
16	Nitrogen	6.037	6.028	-0.008
17	Oxygen	7.558	7.411	-0.147
18	Oxygen	7.550	7.398	-0.152
19	Oxygen	7.328	7.381	0.053
20	Oxygen	7.401	7.415	0.014

21	Oxygen	7.592	7.401	-0.191
22	Oxygen	7.463	7.398	-0.065
23	Oxygen	7.321	7.416	0.096
24	Oxygen	7.347	7.412	0.064
25	Oxygen	7.543	7.503	-0.040
26	Phosphorus	1.693	1.913	0.220
27	Phosphorus	1.737	1.912	0.175
28	Phosphorus	1.758	1.837	0.079
	Total	98.000	98.002	

Table S3. The valence Bader charges of DETMP before and after adsorption on Barite

#	Element	Before Adsorption	After adsorption	Charge Difference
1	Carbon	3.769	3.701	-0.068
2	Carbon	3.650	3.720	0.070
3	Carbon	3.714	3.773	0.059
4	Carbon	3.785	3.674	-0.111
5	Carbon	4.156	4.121	-0.035
6	Carbon	4.189	4.155	-0.034
7	Carbon	4.116	4.218	0.102
8	Carbon	4.069	4.158	0.089
9	Carbon	4.088	4.200	0.112
10	Hydrogen	0.948	0.962	0.014
11	Hydrogen	0.895	0.947	0.051
12	Hydrogen	0.952	0.946	-0.006

13	Hydrogen	1.013	0.988	-0.024
14	Hydrogen	0.958	0.937	-0.021
15	Hydrogen	0.960	0.923	-0.037
16	Hydrogen	0.924	1.004	0.080
17	Hydrogen	0.952	0.963	0.011
18	Hydrogen	0.930	0.940	0.010
19	Hydrogen	0.958	0.962	0.004
20	Hydrogen	0.843	0.939	0.097
21	Hydrogen	0.924	0.915	-0.010
22	Hydrogen	0.334	0.321	-0.013
23	Hydrogen	0.242	0.302	0.060
24	Hydrogen	0.881	0.840	-0.041
25	Hydrogen	0.889	0.886	-0.004
26	Hydrogen	0.278	0.354	0.076
27	Hydrogen	0.196	0.322	0.126
28	Hydrogen	0.942	0.908	-0.034
29	Hydrogen	0.885	0.902	0.017
30	Hydrogen	0.896	0.861	-0.035
31	Hydrogen	0.902	0.932	0.029
32	Hydrogen	0.264	0.293	0.030
33	Hydrogen	0.316	0.319	0.004
34	Hydrogen	0.338	0.305	-0.033

35	Hydrogen	0.347	0.269	-0.078
36	Hydrogen	0.267	0.294	0.027
37	Hydrogen	0.362	0.283	-0.079
38	Nitrogen	5.960	5.977	0.017
39	Nitrogen	5.996	5.944	-0.052
40	Nitrogen	5.964	5.996	0.032
41	Oxygen	7.447	7.441	-0.006
42	Oxygen	7.621	7.381	-0.240
43	Oxygen	7.413	7.410	-0.004
44	Oxygen	7.566	7.394	-0.172
45	Oxygen	7.571	7.366	-0.205
46	Oxygen	7.493	7.408	-0.085
47	Oxygen	7.540	7.403	-0.136
48	Oxygen	7.481	7.417	-0.063
49	Oxygen	7.521	7.400	-0.121
50	Oxygen	7.338	7.394	0.056
51	Oxygen	7.581	7.418	-0.163
52	Oxygen	7.289	7.451	0.162
53	Oxygen	7.458	7.443	-0.015
54	Oxygen	7.544	7.433	-0.111
55	Oxygen	7.489	7.462	-0.026
56	Phosphorus	1.699	1.854	0.155

57	Phosphorus	1.734	1.922	0.188
58	Phosphorus	1.703	1.863	0.160
59	Phosphorus	1.751	1.812	0.060
60	Phosphorus	1.711	1.898	0.187
	Total	194.000	194.026	